ORIGINAL RESEARCH

Disruption of VEGF Mediated Flk-1 Signaling Leads to a Gradual Loss of Vessel Health and Cardiac Function During Myocardial Infarction: Potential Therapy With Pellino-1

Mahesh Thirunavukkarasu, PhD;* Vaithinathan Selvaraju, PhD;* Mandip Joshi, MD;† Vladimir Coca-Soliz, MD;† Leonidas Tapias, MD;† IbnalWalid Saad, MD; Craig Fournier, MD; Aaftab Husain, MD; Jacob Campbell, DO, MPH; Siu-Pok Yee, PhD; Juan A. Sanchez, MD, FACS; J. Alexander Palesty, MD, FACS; David W. McFadden, MD, FACS; Nilanjana Maulik, PhD, FAHA

***Background*—**The present study demonstrates that the ubiquitin E3 ligase, Pellino-1 (Peli1), is an important angiogenic molecule under the control of vascular endothelial growth factor (VEGF) receptor 2/Flk-1. We have previously reported increased survivability of ischemic skin flap tissue by adenovirus carrying Peli1 (Ad-Peli1) gene therapy in Flk-$1^{+/-}$ mice.

***Methods and Results*—**Two separate experimental groups of mice were subjected to myocardial infarction (MI) followed by the immediate intramyocardial injection of adenovirus carrying LacZ (Ad-LacZ) (1×10^9 pfu) or Ad-Peli1 (1×10^9 pfu). Heart tissues were collected for analyses. Compared with wild-type (WTMI) mice, analysis revealed decreased expressions of Peli1, phosphorylated (p-)Flk-1, p-Akt, p-eNOS, p-MK2, p-IκBα, and NF-κB and decreased vessel densities in Flk-$1^{+/-}$ mice subjected to MI (Flk-$1^{+/-}$MI). Mice (CD1) treated with Ad-Peli1 after the induction of MI showed increased β-catenin translocation to the nucleus, connexin 43 expression, and phosphorylation of Akt, eNOS, MK2, and IκBα, that was followed by increased vessel densities compared with the Ad-LacZ–treated group. Echocardiography conducted 30 days after surgery showed decreased function in the Flk$1^{+/-}$MI group compared with WTMI, which was restored by Ad-Peli1 gene therapy. In addition, therapy with Ad-Peli1 stimulated angiogenic and arteriogenic responses in both CD1 and Flk-$1^{+/-}$ mice following MI. Ad-Peli1 treatment attenuated cardiac fibrosis in Flk-$1^{+/-}$MI mice. Similar positive results were observed in CD1 mice subjected to MI after Ad-Peli1 therapy.

***Conclusion*—**Our results show for the first time that Peli1 plays a unique role in salvaging impaired collateral blood vessel formation, diminishes fibrosis, and improves myocardial function, thereby offering clinical potential for therapies in humans to mend a damaged heart following MI. **(*J Am Heart Assoc*. 2018;7:e007601. DOI: 10.1161/JAHA.117.007601.)**

Key Words: adenovirus • animal models • gene therapy • genetics • myocardial infarction • myocardial revascularization

Globally, cardiovascular disease is a leading cause of morbidity and mortality and most commonly presents as coronary artery disease, which is characterized by reduced blood flow to the myocardium.[1] This restriction can lead to ischemic damage and the loss of cardiomyocytes. Current methods of treatment for coronary artery disease primarily aim to reestablish blood flow and reduce the workload of the heart through pharmacological means. However, research

From the Molecular Cardiology and Angiogenesis Laboratory (M.T., V.S., M.J., V.C.-S., L.T., I.S., C.F., A.H., J.C., N.M.), Department of Surgery (M.T., V.S., C.F., A.H., J.C., D.W.M., N.M.), and Center for Mouse Genome Modification (S.-P.Y.), University of Connecticut Health, Farmington, CT; Stanley J. Dudrick Department of Surgery, Saint Mary's Hospital, Waterbury, CT (M.J., V.C.-S., L.T., I.S., J.A.S., J.A.P.).

Accompanying Figures S1 and S2 are available at https://www.ahajournals.org/doi/suppl/10.1161/JAHA.117.007601

*Dr Thirunavukkarasu and Dr Selvaraju contributed equally to this work as co-first authors.

†Dr Joshi, Dr Coca-Soliz, and Dr Tapias contributed equally to this work as co-second authors.

This work was presented at the American Heart Association Scientific Sessions, November 15 to 19, 2014, in Chicago, IL, the American College of Surgeons Annual Clinical Congress, October 4 to 8, 2015, in Chicago, IL, the Annual Surgical Resident and Fellow Research Presentation Day of the New England Surgical Society, May 8, 2015, in Waltham, MA, and the New England Surgical Society Annual Meeting, September 25 to 27, 2015, in Newport, RI.

Correspondence to: Nilanjana Maulik, PhD, FAHA, Molecular Cardiology and Angiogenesis Laboratory, Department of Surgery, University of Connecticut Health, Farmington Avenue, Farmington, CT. E-mail: nmaulik@uchc.edu

Received September 13, 2017; accepted July 20, 2018.

Clinical Perspective

What Is New?

- Disruption of vascular endothelial growth factor signaling by inhibition of Flk-1 inhibits Pellino-1 expression and reduces angiogenic effect and cardiac repair.
- Compared with normal healthy heart, Pellino-1 expression was found to be downregulated in the infarcted myocardium.
- Overexpression of Pellino-1 initiates an angiogenic effect and amelioration of cardiac remodeling following myocardial infarction.
- Deterioration of cardiac repair and increased ventricular remodeling in Flk-1–knockout mice subjected to myocardial infarction was rectified with Pellino-1 treatment.

What Are the Clinical Implications?

- Our work expanded the understanding of a novel molecular mechanism of vascular endothelial growth factor–mediated signaling via a newly identified therapeutic molecule, Pellino-1, in the ischemic myocardium for cardiac repair.

indicates that angiogenesis has the potential for improving long-term treatment of damage caused by myocardial infarction (MI). Various pathways and molecules are involved in the initiation and regulation of angiogenesis, including vascular endothelial growth factor (VEGF), a major architect of this process. VEGF is a potent mitogen specific to endothelial cells and a secreted dimeric protein that is involved in the induction of angiogenesis.[2,3] VEGF follows a tyrosine kinase receptor pathway to promote endothelial cell differentiation and migration.[3] In a previous study, we examined the effect of adenoviral administration of VEGF along with angiopoietin-1 in diabetic mice after the induction of MI.[4] We observed markedly enhanced neovascularization and diminished cardiac fibrosis in the treatment group. We also noted an improved cardiac functions as assessed by echocardiography. However, our interest shifted from VEGF to the molecules downstream of VEGF that may be involved in angiogenesis after clinical trials of VEGF failed to yield similar outcomes in patients with cardiovascular disease.[5-7]

In addition to VEGF, several additional proteins have been identified as having proangiogenic characteristics. Nuclear factor κ-light-chain enhancer of activated B cells (NFκB) is a transcription factor that controls DNA transcription and is involved in cytokine production and cell survival.[8] Phosphorylation of mitogen-activated protein kinase–activated kinase 2 (MK2) has been shown to aid in the activation of NFκB, which, as described above, aids in angiogenesis.[8] Another molecule, the gap junction protein connexin 43 (Cx43), has been implicated in cardioprotection.[9] Inhibiting Cx43 reduces the expression of VEGF in human endothelial progenitor cells by stunting the angiogenic process.[10]

Tyrosine kinase receptor Flk-1, also known as VEGF receptor-2, (VEGFR2), is a major receptor of VEGF. Recently, we have shown increased ischemic skin flap survivability and reduced necrosis by Pellino-1 (Peli1) gene therapy in heterozygous Flk-1 (Flk-$1^{+/-}$)-knockout mice.[11] In an earlier study,[12] we found diminished heart function with the same heterozygous Flk-1/VEGFR2 (Flk-$1^{+/-}$)-knockout mice, even in the presence of ischemic preconditioning (PC). However, the mediating role of VEGF/Flk-1 downstream signaling in the ischemic myocardium during neovascularization remains unclear. Therefore, in the present study we explored the downstream molecular mechanism of VEGF signaling in genetically engineered Flk-$1^{+/-}$ mice subjected to MI and subsequent rescue by the newly identified proangiogenic molecule, Peli1.

Peli1 is 1 of 3 main Pellino molecules from the E3 ubiquitin ligase family. In the immune system, Peli1 is necessary for interleukin 1–mediated activation of NFκB. Peli1 additionally plays a role in Toll-like receptor signaling and negative regulation of T cells.[13] Although the immunological effects of Peli1 have been extensively studied, the involvement of Peli1 in angiogenesis has not yet been examined. Peli1 upregulates MK2 through ubiquitination and activation of inhibitor of apoptosis-2 (IAP2), which in turn facilitates the ubiquitination and degradation of tumor necrosis factor receptor–associated factor-3, a negative regulator of MK2.[14] Peli1 also plays a role in the activation of NFκB.[13] Peli1 mediates activation of IκB kinase (IKK) via the Toll/Interleukin-1 receptor homology-domain-containing adaptor-inducing interferon-β–dependent Toll-like receptor pathway.[15] Interestingly, the phosphoinositide 3-kinase/protein kinase B (PI3K/Akt) pathway functions through IKK in a fashion that promotes the phosphorylation of NFκB.[16,17] Increased phosphorylation of Akt and endothelial nitric oxide synthase (eNOS) promote angiogenesis, likely via IKK in a manner involving NFκB and β-catenin activation.[18]

The present study demonstrates the indispensable role of Peli1 in angiogenic remodeling and cardiac repair using loss of function related to an Flk-$1^{+/-}$ mouse model of MI. We found that a reduction of Flk-1 correlates with decreased expression of Peli1. Therefore, it is possible that Peli1 plays a role in angiogenesis and cardiac repair downstream of VEGF/Flk-1. Given previous knowledge regarding the benefits of triggering the VEGF cascade, the importance of Flk-1, and the finding that the knockdown of Flk-1 downregulates Peli1, we hypothesize that overexpression of Peli1 may protect the heart from ischemic damage after MI, providing a novel target for therapeutic development.

Materials and Methods

The data, analytic methods, and study materials will not be made available to other researchers for purposes of reproducing the results or replicating the procedure because other related projects are in progress.

In Vitro Experiments

Cell Culture

Human umbilical vein endothelial cells (HUVECs) were purchased from Lonza (Walkersville, MD). Cells were maintained in endothelial cell growth medium 2 with supplemental growth factors and antibiotics, per the manufacturer's specifications.[11]

Angiogenic Tube Formation Assay

Control small interfering RNA (C.siRNA; Cat# SC-37007) and siRNA targeted against Peli1 (Peli1.siRNA; Cat# SC-44401) were purchased from Santa Cruz Biotechnology, Inc (Dallas, TX). The HUVECs were treated with either C.siRNA or Peli1.siRNA (60 nmol/L) for 48 hours and then treated with VEGF. Matrigel with reduced serum (Cat# 354230, Corning Incorporated, Corning, NY) was dissolved at 4°C overnight, after which a μ-Slide plate (ibidi USA, Inc, Madison, WI) was prepared with 10 μL Matrigel in each well and incubated at 37°C for 30 minutes. After incubation of the plates, 50 μL of treated cells (1.5×10^5 cells/mL) were seeded onto the gel. Tube formation was assessed after 8 hours of seeding using an Olympus QColor 3TM digital camera mounted on an Olympus BH2 microscope. Each well was photographed at $\times$200 magnification.[11]

Cell Proliferation

The HUVECs underwent siRNA (C.siRNA or Peli1.siRNA) transfection for 48 hours, followed by 8 hours of hypoxia and 24 hours of reoxygenation. Five thousand cells per well were subsequently seeded onto a 96-well plate and followed for 0, 24, and 48 hours. A CyQUANT cell proliferation assay was performed as per the manufacturer's instructions (Cat# C7026, Molecular Probes, Thermo Fisher Scientific, Waltham, MA).

Wound Assay

HUVECs that underwent siRNA transfection for 48 hours (C.siRNA or Peli1.siRNA) in 12-well plates, followed by 8 hours of hypoxia and 24 hours of reoxygenation, were allowed to reach 90% confluence. Uniform wounds were created with a sterile 200-μL pipette tip in the HUVECs monolayer and supplemented with fresh EBM-2 medium with reduced serum (n=3-4/group). Wounds were imaged at 0, 3, 6, 12, 24, and 36 hours using the $\times$4 objective of an inverted microscope (iRis Digital Cell Imaging System, Logos Biosystems, Annandale, VA). The wound area was calculated from each image using ImageJ software (NIH, Bethesda, MD), and wound closure (%) was calculated using a previously reported formula.[11,19,20]

In Vivo Experiments

Animals

This study was executed in compliance with the standards of laboratory animal care designed by the National Society for Medical Research in compliance with the *Guide for the Care and Use of Laboratory Animals* prepared by the National Academy of Sciences and published by the National Institutes of Health (publication No. 85-23, revised 1985). Our experimental protocol was approved by the Institutional Animal Care and Use Committee of the University of Connecticut Health Center (Farmington, CT). Male CD1/ICR mice (8-12 weeks of age) were purchased from Envigo (Indianapolis, IN) for use in this experiment. Heterozygous (Flk-$1^{+/-}$) mice (strain: B6.129-Kdrtm1Jrt/J) were purchased from Jackson Laboratory (Bar Harbor, ME) and backcrossed with ICR mice for 10 generations for use in this experiment.

Mouse Model of MI and Gene Therapy

Mice from 8 to 12 weeks of age were used in this study. All mice were anesthetized, intubated, and positioned for surgery. Anesthesia was accomplished through intraperitoneal administration of ketamine hydrochloride (100 mg/kg) and xylazine (10 mg/kg). We also administered the antibiotic cefazolin (25 mg/kg) prophylactically. After anesthesia, the mice were intubated and ventilation was initiated (150 strokes/min, stroke volume of 300 μL) using a rodent ventilator (model 845; Harvard Apparatus, Holliston, MA). The mice were then placed in a right decubitus position to expose the left side of the chest wall for left lateral thoracotomy. The fur was removed from the left chest wall area using commercial hair removal cream (Nair® lotion with cocoa butter and vitamin E), and the incision area was cleaned with a 70% isopropyl alcohol prep pad followed by betadine application.

During the operative phase, an incision was made at the fourth intercostal region, and a left lateral thoracotomy was performed. The muscles and fascia were separated using a blunt dissection and portable electrocautery (HIT1 Change-A-Tip™; Bovie Medical Corp, Clearwater, FL) to enter the left thoracic cavity and expose the heart. The left anterior descending coronary artery (LAD) was visualized, and an 8-0 prolene suture with a tapered needle was used for ligation. To induce permanent MI, the needle and suture were passed under the LAD just below the edge of the left atrium and ligated. Visual evidence of pale color distal to the occlusion point, indicating decreased blood flow, was used to ensure that the occlusion was successful. In sham-treated animals,

the needle and suture were passed under the LAD and removed without ligation of the artery. The thoracotomy and skin were then closed in normal operative fashion.

For the gene therapy experiments, we administered the adenoviral vectors (Ad) carrying LacZ or Peli1 immediately after the MI or sham surgical procedure. Mice in the Ad-Peli1 treatment groups were administered an adenoviral vector encoding Peli1 (1×10^9 pfu), and those in the Ad-LacZ treatment (1×10^9 pfu) groups were administered an adenoviral vector encoding LacZ. Mice in each treatment group were injected with adenovirus (in 50 μL of PBS) at 4 locations in the peri-infarct region known as the "high-risk area" using a 30-gauge needle (12.5 μL injected at each location). The apex of the left ventricle (LV) was excluded as a site of administration because this area bears a higher risk of the needle entering the ventricle and releasing adenovirus into general circulation. After administration of the adenovirus, the incision was closed.

The surgical area was cleaned with Betadine after the skin was closed to prevent infection. Buprenorphine (0.05-0.1 mg/kg) was also postoperatively and subcutaneously administered for pain management. The mice were weaned off the ventilator and placed on a heating pad to recover from anesthesia. The mice were subsequently placed on a pain-management schedule that included receiving buprenorphine (0.05-0.1 mg/kg) every 12 hours for 3 days.[21]

We modified the previously described method to conduct preconditioning (PC) in mice (PC limits infarct size following regional ischemia-reperfusion in in situ mouse hearts). Briefly, the LAD was identified after intubation and thoracotomy, and an 8-0 prolene suture was passed underneath. A small piece of tubing was placed on the myocardial surface, and the suture was tied around the tubing. After 4 minutes, the tied knots were released. We repeated this process for 4 cycles; each cycle comprised 4 minutes each of ischemia and reperfusion. After the fourth cycle of reperfusion, the LAD was permanently ligated, the chest was closed, and the animal was allowed to recover before extubation.[22]

Experimental Groups and Treatments

For experiments involving Flk-$1^{+/-}$ mice, the animals were divided into 4 groups: (1) sham-operated wild-type (WTS) mice, (2) wild-type MI (WTMI) mice, (3) Flk-$1^{+/-}$S, and (4) Flk-$1^{+/-}$MI. Another set of CD1 mice was divided into 4 groups for gene therapy experiments: (1) Ad-LacZ sham (Ad-LacZS), (2) Ad-LacZMI, (3) Ad-Peli1 sham (Ad-Peli1S), and (4) Ad-Peli1MI. In the rescue experiments, Flk-$1^{+/-}$ mice were subjected to MI and treated with Ad-LacZ (Flk-$1^{+/-}$MI+Ad-LacZ group) or Ad-Peli1 (Flk-$1^{+/-}$MI+Ad-Peli1 group). Tissue sections from the peri-infarct region of the LV were resected, flash-frozen in liquid nitrogen, and stored at −80°C for molecular analysis. For immunohistochemistry analyses, hearts were removed and the tissues sectioned transversely and fixed overnight in 10% buffered formalin for paraffin sections. For these assays, heart tissues were harvested 4 and 7 days after surgery. Tissues were also collected 30 days after surgery for immunohistochemical analysis and to measure the extent of myocardial fibrosis by PicroSirius Red staining. Echocardiography was performed 30 days after surgery to measure heart function before tissues were harvested.

Electrophoretic Mobility Shift Assay

An electrophoretic mobility shift assay was performed per the manufacturer's instructions (Gel-Shift Assay System, Promega, Madison, WI)[12] to measure NFκB binding activity in the myocardium 8 hours after MI.

Quantitative Real-Time PCR

RNA was isolated (Cat# 74104, RNeasy Mini Kit, Qiagen Inc, Valencia, CA) from LV heart tissue collected 8 hours after MI, per the manufacturer's instructions. One microgram of RNA was used to synthesize cDNA (Cat# 17008891, iScript cDNA synthesis kit, BioRad, Hercules, CA). Quantitative polymerase chain reaction (PCR) was performed to measure the relative expression of the *Peli1* gene, as previously described.[23] β-Actin was used as a reference gene to normalize the measured expression of *Peli1*. Primer sequences used for quantitative PCR were as follows: forward primer 5′-AGAGGAAAGATGGTGGAAAT-3′ and reverse primer 5′-CAG-TAGGAGTATGGGAAAGG-3′.

Immunohistochemistry for Capillary and Arteriolar Densities and the Expression of Cx43

To measure capillary and arteriolar densities, heart tissues collected after surgery were fixed overnight in 10% buffered formalin (Sigma-Aldrich, St. Louis, MO) followed by 70% ethanol and embedded in paraffin blocks. Tissue sections of 5 μm thick were made using Shandon Colorfrost Plus slides (Cat# 9991001, Thermo Fisher Scientific, Waltham, MA). The sections were deparaffinized, rehydrated through a 100% to 70% alcohol gradient, and blocked with 2.5% normal horse serum (Cat# S-2012, Vector Laboratories Inc, Burlingame, CA). To measure capillary density, the sections were stained with rabbit anti-CD31 (1:100 in PBS; Cat# ab28364, Abcam Inc, Cambridge, MA). We used an ImmPRESS anti–rabbit Ig (peroxidase) kit (Cat# MP-7401, Vector Laboratories Inc, Burlingame, CA) for the secondary antibody. A 3,3′-diaminobenzidine staining kit (peroxidase substrate kit diaminobenzidine, Cat# SK-4100, Vector Laboratories, Burlingame, CA) was used for chromogenic visualization of antibody binding.

Digital images were taken at ×400 magnification using an Olympus BH2 microscope and used to quantify capillary density. Counts (per 1 mm^2) were made in the area at risk after superimposing a calibrated morphometric grid on each image using Adobe Photoshop CS4 software (Adobe Systems, San Jose, CA).

To estimate arteriolar density, tissue sections were counterstained with mouse anti–α-smooth muscle actin (1:100 in PBS; Cat# ab7817, Abcam Inc, Cambridge, MA). The tissue sections were then incubated with donkey anti-mouse secondary antibody labeled with Alexa Fluor 488 (1:200 in PBS; Invitrogen, Carlsbad, CA) for 1 hour at room temperature. The sections were mounted with a coverslip using Vectashield fluorescent mounting medium (Vector Laboratories Inc, Burlingame, CA). Tissue images were taken using an Olympus BX53 microscope with an Olympus DP73 digital color camera attached to it. Images were acquired and diameter was measured using CellSens Dimension (version 1.6) software. The arteriolar density observed in each image was expressed as the count per 1 mm^2.

Immunohistochemistry for Cx43 expression was performed only for mice in the Ad-LacZMI and Ad-Peli1MI groups. Mice were euthanized 4 days after the induction of MI and gene therapy. The hearts were removed, and tissue sections were embedded in paraffin blocks as described above. The sections were stained using anti–rabbit Cx43 (1:100 in PBS; Cat# C6219, Sigma-Aldrich, St. Louis, MO) and anti–mouse cTnT (1:200 in PBS; Cat# ab8295, Abcam Inc, Cambridge, MA). The sections were then incubated with goat anit-rabbit labeled with Alexa Fluor 488 (1:200 in PBS; Cat# A11034; Invitrogen, Carlsbad, CA) for Cx43 and donkey anti-mouse labeled with Alexa Fluor 555 (1:200 in PBS; Cat# A31570, Invitrogen, Carlsbad, CA) for cTnT. TO-PRO-3 Iodide (Cat# T3605, Invitrogen, Carlsbad, CA) was added for nuclear staining. Tissue images were taken using a Zeiss LSM510 Meta confocal microscope. The arteriolar density observed in each image was expressed as the count per 1 mm^2.

Immunohistochemistry to Measure the Transfection Efficiency of Ad-LacZ and Ad-Peli1

To ensure that our gene-transfer technique was effective in vivo, adenovirus gene expression was evaluated in the sham-operated control groups 4 days after treatment. Hearts were exposed by left lateral thoracotomy using the method described above and injected with either Ad-Peli1 or Ad-LacZ at 4 sites. Four days later, the mice were euthanized, and the hearts were removed and fixed overnight in 10% formaldehyde, followed by paraffin embedding. Sections 5 μm thick were deparaffinized using 2× washes of Histo-Clear (National Diagnostics, Atlanta, GA). They were then rehydrated in an alcohol gradient in the order of 2× 100%, 90%, 80%, and 70%, for 5 minutes each. The sections were washed 3 times in PBS and then in antigen retrieval buffer (Cat# S1699, Dako, Santa Clara, CA). Next, endogenous peroxidase was blocked using 0.3% hydrogen peroxide in PBS for 30 minutes. By use of a buffered casein solution (Power Block™ universal blocking reagent; Cat# HK085-5K, Bio Genex, San Ramon, CA), nonspecific binding sites were then blocked at room temperature for 8 minutes. The slides were washed again 3 times in PBS and then stained for Peli1 using anti–Pellino-1 antibody (1:100 dilution in PBS; Cat# SC-31619, Santa Cruz Biotechnology Inc, Dallas, TX) overnight at 4°C followed by incubation with anti-goat secondary antibody labeled with Alexa Fluor 488 (1:200 dilution; Cat# A11055; Invitrogen, Carlsbad, CA) for 1 hour. Nuclei were counterstained with TO-PRO-3 Iodide. Slides were washed and mounted with Fluoromount™ and visualized using a Zeiss LSM 510 Meta confocal microscope.

Western Blot Analysis of Peli1, p-Flk-1, p-MK2, p-eNOS, p-Akt, p-IκBα and β catenin

The peri-infarct region of the LV was collected either 24 hours or 4 days after surgery, flash-frozen in liquid nitrogen, and stored at −80°C for Western blot analysis. To quantitatively analyze the expressions of various proteins, we used the SDS-PAGE Western blot technique. Tissue samples were homogenized using CelLytic™ NuCLEAR™ Extraction Kit (Sigma-Aldrich, St. Louis, MO). The cytosolic and nuclear protein was separated, and the protein concentration was established using a bicinchoninic acid protein assay kit (Pierce, Rockford, IL). Ten-percent polyacrylamide gels were used for electrophoresis for Peli1, p-MK2/MK2, p-AKT/AKT and p-IκBα/IκBα, and 7.5% gels were used for p-Flk-1/Flk-1, p-eNOS/eNOS and β-catenin (cytosolic). β-catenin from nuclear protein fraction was separated using 4–15% gels. GAPDH, β-actin, Vinculin or Histone-H3 was used as a loading control. In addition, each protein's dephosphorylated form was used as a second loading control for each protein. The p-Flk-1 (1:1000 dilution; Cat# ab194806), Flk-1 (1:1000 dilution; Cat# ab39256), p-MK2 (1:500 dilution; Cat# 3041), MK2 (1:500 dilution, Cat# 3042), p-eNOS (1:1000 dilution; Cat# 9571), eNOS (1:1000 dilution; Cat# 9572), p-Akt (1:1000 dilution; Cat# 9271), and Akt (1:1000 dilution; Cat# 9272) antibodies were purchased from Cell Signaling Technology (Danvers, MA). p-IκBα (1:1000 dilution; Cat# ab47752), anti-vinculin (1:1000; Cat# ab18058) was purchased from Abcam Inc (Cambridge, MA), and the IκBα (1:1000 dilution; Cat# SC-847), β-catenin (1:1000 dilution; Cat# SC-7963) and Histone H3 (1:1000 dilution; Cat# SC-10809) antibody was purchased from Santa Cruz Biotechnology, Inc (Dallas, TX). The GAPDH antibody (1:4000 dilution, Cat# AM4300) and anti–β-actin (1:2000 dilution, Cat# A5441) was purchased from Thermo Fisher Scientific (Waltham, MA) and Sigma-Aldrich, St. Louis,

MO), respectively. The Peli1 antibody (1:1000 dilution; Cat# ab13812) was purchased from Abcam Inc (Cambridge, MA). Visualization of the primary antibody was achieved using the respective horseradish peroxidase–conjugated secondary antibodies and enhanced chemiluminescence.

Histochemical Staining to Determine the Extent of Myocardial Fibrosis

To measure the extent of myocardial fibrosis, paraffin-embedded sections of the heart were stained using PicroSirius Red (Cat# 365548, Sigma-Aldrich, St. Louis, MO). The paraffin-embedded sections were then deparaffinized using Histo-Clear (National Diagnostics, Atlanta, GA) and rehydrated using an alcohol gradient (2× 100%, followed by 90%, 80%, and 70%). The sections were washed in distilled water and stained with PicroSirius Red for 1 hour before being washed twice in acidified water for 3 minutes each. The slides were then placed twice in 100% alcohol and Histo-Clear and mounted using Permount mounting medium (Thermo Fisher Scientific, Waltham, MA). Tissue images were taken at ×400 magnification using an Olympus BH2 microscope. ImageJ software (NIH, Bethesda, MD) was used to measure the degree of fibrosis.

Echocardiography

Thirty days after the induction of MI, the mice were sedated using isoflurane (3% inhaled). The mice were secured with tape to a custom mold in a supine position to maintain a natural body shape, and the fur was removed from the chest wall using commercial hair removal cream (Nair® lotion with cocoa butter and vitamin E). Ultrasound gel was spread over the chest, and an ultrasound biomicroscopy (Vevo 770, Visual-Sonics Inc, Toronto, ON, Canada) with a 25-MHz transducer was used for imaging. Left ventricular imaging was performed in the apical, parasternal long-axis, and parasternal short-axis views for assessments of systolic function, cavity diameter, diastolic function, and LV end-systolic and end-diastolic volumes. Two-dimensional directed M-mode images of the short axis of the LV were taken inferior to the level of the papillary muscles for assessments of chamber diameter. All parameters were calculated in accordance with modified American Society of Echocardiography recommended guidelines.

Statistical Analysis

Data were analyzed using Graph-Pad Prism software, Version 5 (San Diego, CA). All results are expressed as the mean±standard error of the mean or median and interquartile range, as mentioned in the figure legends. Statistical comparisons between 2 groups were made using unpaired t tests or Mann-Whitney U test. For statistical comparisons of more than 2 groups, 1-way ANOVA followed by Bonferroni post hoc tests were used. We also used the Kruskal-Wallis nonparametric test when the sample size differed between the groups. To analyze the proliferation and wound closure data, we used 2-way repeated-measure ANOVA followed by a Bonferroni post hoc test. Differences were considered statistically significant if $P<0.05$.

Results

Decreased Phosphorylation of Flk-1, Akt, eNOS, MK2, IκBα Levels, and NFκB Activity in Flk-1$^{+/-}$ Mice After MI

Western blot analysis and gel-shift assays were performed in Flk-1$^{+/-}$ mice, 8 and 24 hours after surgery to evaluate molecular changes associated with VEGF-related downstream molecules, including Flk-1, Akt, eNOS, MK2, IκBα, and NFκB. Heterozygous Flk-1$^{+/-}$ mice (Flk-1 reduced to 50%)[12] subjected to MI revealed 2.4-fold reduced Flk-1 expression compared with WTMI and 3.9-fold reduced expression compared with WTS mice. In addition, the WTMI group clearly showed a prominent reduction (1.62-fold) in Flk-1 expression compared with the WTS. Flk-1 expression was normalized with vinculin (mol wt 130 kDa) as a loading control. Reduced phosphorylation of Flk-1 (p-Flk-1/Flk-1 ratio) was readily detectable in both the WTMI (1.5-fold) and Flk-1$^{+/-}$MI (2.3-fold) groups compared with WTS. There was also a significant difference in phosphorylation of Flk-1 expression (p-Flk-1/Flk-1) in the Flk-1$^{+/-}$MI group (1.6-fold) compared with WTMI (Figure 1A and 1F). We also investigated the effect of downregulation of Flk-1 on Akt and eNOS expression (both nonphosphorylated and phosphorylated forms) because PI3K/Akt/eNOS signaling is known to play an important role downstream of Flk-1 (VEGFR2).[24-27] Akt phosphorylation at the Ser 473 site was significantly reduced in both the WTMI (1.6-fold) and Flk-1$^{+/-}$MI (6.1-fold) groups compared with WTS. When the extent of phosphorylation of Akt between the MI groups was examined, Akt was found to have less detectable phosphorylation (3.6-fold) in the Flk-1$^{+/-}$MI group compared with the WTMI group (Figure 1B and 1G). Again, inhibition of Flk-1 abolished Ser 1177 phosphorylation of eNOS in both Flk-1$^{+/-}$MI (2.5-fold) and WTMI (1.6-fold) mice compared with WTS mice. Noticeable inhibition of eNOS phosphorylation was also observed in the Flk-1$^{+/-}$MI group (1.6-fold) compared with the WTMI group (Figure 1C and 1H).

Consistent with these findings, our results revealed a reduction in phosphorylation of MK2 and IκBα in the WTMI group (0.76±0.02 and 0.20±0.1, respectively) compared with WTS (0.90±0.02 and 0.83±0.24, respectively). Significant reductions in both p-MK2 and p-IκBα levels were observed in the Flk-1$^{+/-}$MI group (0.57±0.05 and 0.04±0.01) compared with WTMI (Figure 1D, 1E, 1I, and 1J). As shown in Figure 1K, the gel-shift assay demonstrated

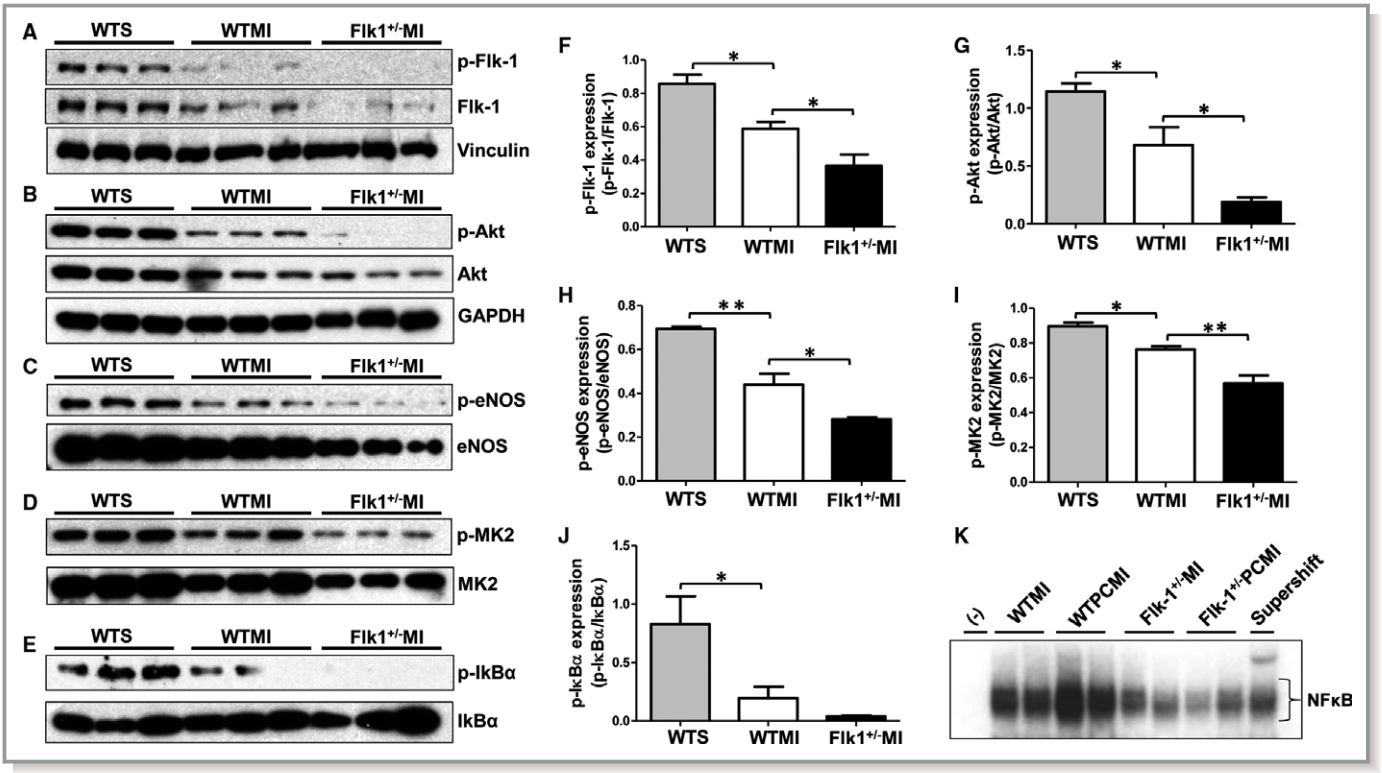

Figure 1. Flk-1 inhibition reduces phosphorylation of Flk-1, Akt, eNOS, MK2, IκBα, and NFκB activity after induction of MI. A, Western blot analysis of p-Flk-1, (B) p-Akt, (C) p-eNOS, (D) p-MK2, and (E) p-IκBα proteins in WTS, WTMI, and Flk-$1^{+/-}$MI groups (24 hours after surgery). F through J, Bar graphs represent (F) p-Flk-1, (G) p-Akt, (H) p-eNOS, (I) p-MK2, and (J) p-IκBα levels normalized to their respective total protein levels. The Flk-$1^{+/-}$MI group showed reduced levels of p-Flk-1, p-Akt, p-eNOS, p-MK2, and p-IκBα expression compared with the WTMI group. Values are mean±SEM (n=3/group) (*P<0.05, **P<0.01). K, Electrophoretic mobility shift assay of NFκB activation (8 hours after surgery). NFκB activity was reduced in the Flk-$1^{+/-}$MI group compared with the WTMI group. Flk-$1^{+/-}$MI indicates Flk-$1^{+/-}$ mice subjected to MI; MI, myocardial infarction; p-, phosphorylated; PC, ischemic preconditioning; WT, wild type; the minus symbol (−) represents the negative control; WTMI, WT mice subjected to MI; WTS, WT mice subjected to sham surgery.

increased NFκB activity in the ischemic PC WT group (WTPCMI) compared with the non-PC group. However, NFκB activity was drastically reduced in the Flk-$1^{+/-}$MI group compared with WTMI. The Flk-$1^{+/-}$PCMI group also showed reduced NFκB levels compared with WTPCMI, clearly demonstrating that PC-mediated NFκB signaling is abolished in Flk-$1^{+/-}$ mice. Taken together, these results indicate that Flk-1/Akt/eNOS/MK2/IκBα/NFκB is one of the primary mechanism involved in VEGF/Flk-1 signaling.

Heterozygous Flk-1 Knockout Mice Show Decreased Vascularization and Cardiac Function and Increased Cardiac Fibrosis

Capillary densities of both WT and Flk-$1^{+/-}$ mice heart sections were analyzed 7 days after surgery by CD31 staining (n=4-5/group). Flk-$1^{+/-}$ mice subjected to sham surgery (Flk-$1^{+/-}$S) showed a significant reduction in capillary density (2239±80.56 counts/mm^2) compared with WTS mice (3226±223.9 counts/mm^2), demonstrating a deleterious effect of reduced Flk-1 (inhibition) on vessel density. The WTMI group also showed a reduction in capillary density (2450±245.1 counts/mm^2) compared with the WTS group (3226±223.9 counts/mm^2), indicating an effect of MI on collateral growth. Within the Flk-$1^{+/-}$groups, the Flk-$1^{+/-}$MI group (1713±54.90 counts/mm^2) exhibited a significant reduction in capillary density compared with the Flk-$1^{+/-}$S group (2239±80.56 counts/mm^2); this finding further confirms the cumulative detrimental effects on vasculogenesis arising from the partial deletion of Flk-1 in Flk-$1^{+/-}$MI mice. Moreover, within the MI groups, Flk-$1^{+/-}$MI mice showed a significant reduction in capillary density (1713±54.90 counts/mm^2) compared with WTMI (2450±245.1 counts/mm^2) (Figure 2A and 2B).

Arteriolar density was analyzed 30 days after surgery in WT and Flk-$1^{+/-}$ mice by α-smooth muscle actin staining (n=6/group) (Figure 2C and 2D). Arterioles were measured and divided into 3 categories based on their diameter: small (11-50 μm), medium (51-75 μm), and large vessels (≥76 μm) (Figure S1). We observed a significant reduction in the density (numbers) of small vessels in the Flk-$1^{+/-}$S group (27.64±1.09 counts/mm^2) compared with the WTS group (38.15±0.29 counts/mm^2). The WTMI (32.02±0.63 counts/

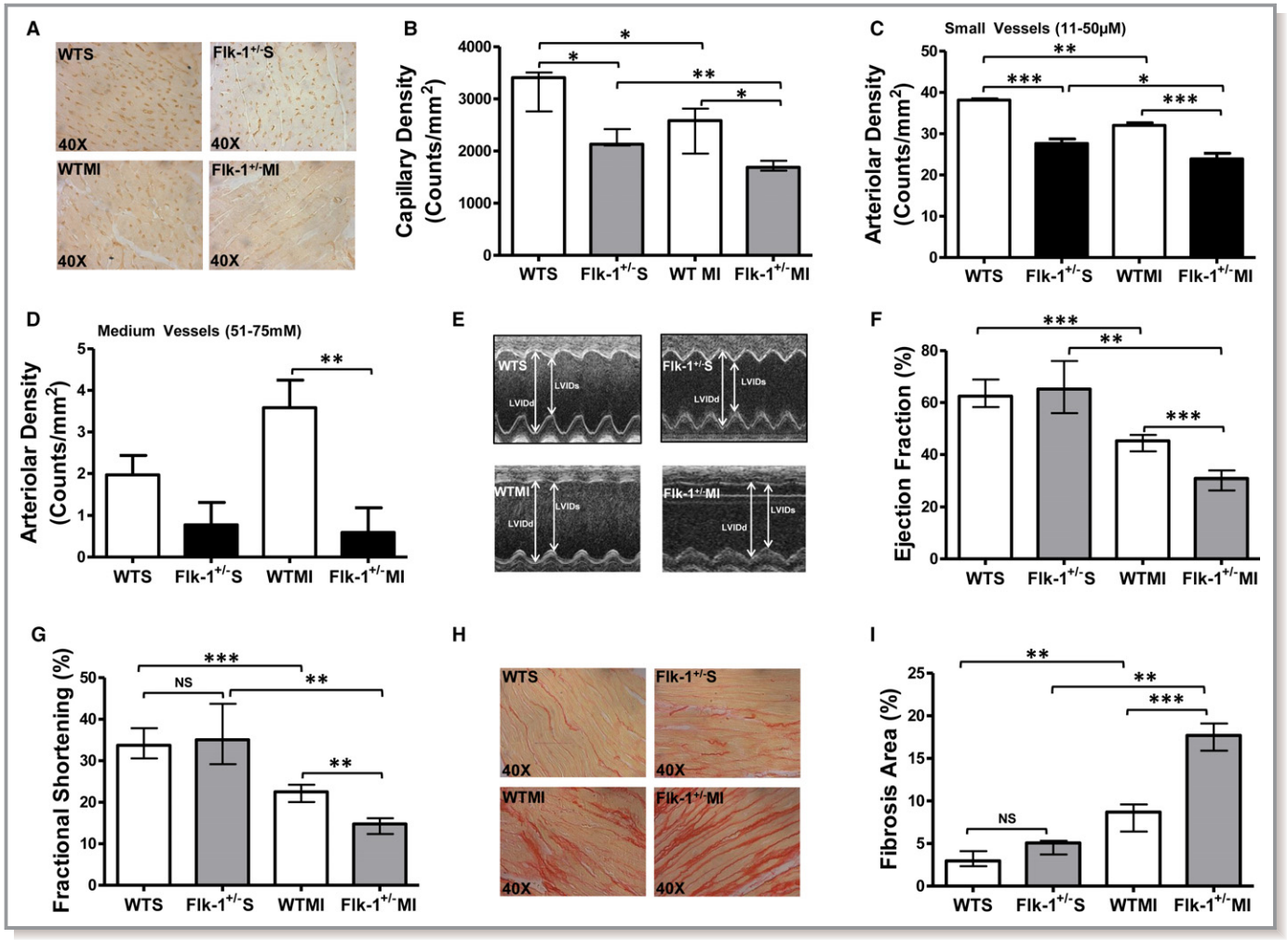

Figure 2. Flk-1 inhibition results in reduced vessel densities and cardiac function along with increased myocardial fibrosis. A, Representative images of CD31 staining for capillary density in different experimental groups (7 days after surgery). B, Bar graph represents the quantitative analysis of capillary density in counts/mm^2. Flk-1$^{+/-}$ mice had a reduced capillary density compared with the WT mice in both sham and MI groups. Values in the bar graph represent median and IQR, (n=4-6/group), (*P<0.05, **P<0.01). C and D, Bar graphs represent arteriolar densities of (C) small and (D) medium-sized arterioles in counts/mm^2 (30 days after surgery). The density of arterioles was reduced in the Flk-1$^{+/-}$MI group compared with the WTMI group. Values are mean±SEM (n=6/group) (*P<0.05, **P<0.01, ***P<0.001). E, Representative M-mode pictures of echocardiographic analysis in different experimental groups. F and G, Measurements of cardiac function by echocardiographic analysis. The bar graphs represent (F) EF and (G) FS measurements (30 days after surgery). Measurements of cardiac function showed that both EF and FS were decreased in Flk-1$^{+/-}$MI mice compared with WTMI. There was no difference between the sham groups in either EF or FS measurements. Values in the bar graphs represent median and IQR, (n=6-10/group), (**P<0.01, ***P<0.001). H, Representative pictures of fibrosis by PicroSirius Red staining in different experimental groups. I, Quantitative analysis of myocardial fibrosis (30 days after surgery). The Flk-1$^{+/-}$MI group showed increased fibrosis compared with the WTMI group. Values in the bar graphs represents median and IQR (n=4-9/group) (**P<0.01, ***P<0.001). EF indicates ejection fraction; Flk-1$^{+/-}$MI, Flk-1$^{+/-}$ mice subjected to MI; Flk-1$^{+/-}$S, Flk-1$^{+/-}$ mice subjected to sham surgery; FS, fractional shortening; IQR, interquartile range; MI, myocardial infarction; S, sham surgery; SEM, standard error of the mean; WT, wild type; WTMI, WT mice subjected to MI; WTS, WT mice subjected to sham surgery.

mm^2) group showed a similarly decreased arteriolar density compared with WTS. However, the Flk-1$^{+/-}$MI group (23.90±1.38 counts/mm^2) exhibited significantly fewer small-sized arterioles compared with WTMI (Figure 2C). Counts of medium-sized vessels for arteriolar density were also significantly lower in the Flk-1$^{+/-}$MI group (0.59 counts/mm^2) compared with WTMI (3.59 counts/mm^2). Although the Flk-1$^{+/-}$S group demonstrated a reduction in medium-sized arterioles compared with the WTS group, this difference did not reach statistical significance (Figure 2D). We did not observe any difference in numbers related to large-sized arterioles in either Flk-1$^{+/-}$S or Flk-1$^{+/-}$MI mice 30 days after MI surgery.

The preoperative echocardiographic analysis performed to measure cardiac function showed no significant difference between WT and Flk-1$^{+/-}$ mice (n=10/group) in either ejection fraction (EF; 65±1.2% and 66±1.8%) or fractional

shortening (FS; 35±0.9% and 35±1.3%). Similarly, no significant difference was observed between the WTS and Flk-$1^{+/-}$S groups in either EF (63±2% versus 65±3.3%) or FS (34±1.4% versus 35±2.5%) 30 days after surgery. However, both the WTMI and Flk-$1^{+/-}$MI groups demonstrated significantly impaired cardiac function compared with their respective sham groups. The Flk-$1^{+/-}$MI group also showed significant reductions in EF and FS (30±1.9% and 14±1.0%, respectively) compared with the WTMI group (44±1.2% and 22±0.7%, respectively) (Figure 2E through 2G). PicroSirius Red staining was performed on cardiac tissues collected from WTMI and Flk-$1^{+/-}$MI mice to observe changes in the distributions of collagen in the LV (Figure 2H and 2I). The bar graphs in Figure 2I show the distribution of collagen in LV tissues of mice from the WTMI and Flk-$1^{+/-}$MI groups. Quantitative analysis of the fibrotic area indicate that fibrosis was more extensive in the Flk-$1^{+/-}$MI group (17.51±1.09%) compared with the WTMI group (8.37±0.79%). No difference in fibrosis was detected between the sham groups.

Peli1 is Negatively Regulated in Heterozygous Flk-1 Knockout Mice Following MI

To determine the impact of Flk-1–mediated Peli1 regulation, the LV risk areas were collected from WTMI and Flk-$1^{+/-}$ mice (n=5-7/group) 8 hours and 4 days after the induction of MI and analyzed for Peli1 expression at the mRNA and protein levels using quantitative real-time PCR (Figure 3A) and Western blot analysis, respectively (Figure 3B and 3C). mRNA expression of Peli1 was significantly downregulated in the Flk-$1^{+/-}$MI group (0.3±0.19-fold) compared with the WTMI group (Figure 3A). Western blot analysis for Peli1 in tissue samples collected from WTMI and Flk-$1^{+/-}$MI mice confirmed that Peli1 protein expression was substantially decreased in the Flk-$1^{+/-}$MI group (2.3-fold) compared with WTMI (Figure 3B and 3C). At the baseline level also, we observed reduced expression of Peli1 in Flk-$1^{+/-}$ mice (1.5-fold) compared with WT. We also examined Peli1 protein expression in 3 different conditions: in the normal heart, control heart subjected to sham surgery (CS), and after the MI procedure (CMI). A significant decrease in Peli1 expression after MI was observed in CMI hearts compared with CS or normal healthy hearts, revealing an important function for Peli1 in cardiovascular disease (Figure 3D). We did not observe any difference of Peli1 expression between CS and normal healthy heart.

Deletion of Peli1 Inhibits Proangiogenic Function in HUVECs: In Vitro Tube Formation, Proliferation, and Wound-Closure Assay

To explore the proangiogenic properties of Peli1, HUVECs were treated with C.siRNA or Peli1.siRNA for 48 hours. Peli1.siRNA-treated HUVECs showed 90% knockdown of Peli1 expression after 48 hours compared with C.siRNA (Figure 3E). The cells were treated with C.siRNA and Peli1.siRNA and were seeded over a Matrigel (Corning Incorporated, Corning, NY) layer with and without VEGF after 48 hours. Six hours after the cells were plated on the Matrigel, the function of HUVEC endothelial tube formation was quantified by counting the total number of endothelial branch points. The HUVECs treated with C.siRNA in the presence of VEGF (C.siRNA+VEGF) showed more endothelial branch points (19.64±0.65) than the group treated with C.siRNA alone (10.33±0.58). Peli1.siRNA abolished the VEGF-induced increase in tube formation, as represented by fewer branch points (2.56±0.78). These data confirm that the complete knockdown of Peli1 in HUVECs has a detrimental effect on endothelial tube formation, even in the presence of VEGF (Figure 3F and 3G). Similar results were observed following an endothelial tube formation assay that replaced the VEGF stimulus with hypoxia/reoxygenation (H/R). Following exposure to H/R, HUVECs treated with C.siRNA showed a significant increase in endothelial branch points compared with those treated with C.siRNA alone (7.13±0.57 versus 2.56±0.29). The H/R-mediated increase in endothelial branch points was inhibited in the presence of Peli1.siRNA (0.53±0.14) (Figure 3H and 3I).

A fluorescence DNA quantification assay was performed using a CyQUANT kit to assess the effect of Peli1-mediated cell proliferation. The HUVECs treated with either C.siRNA or Peli1.siRNA for 48 hours were collected and uniformly reseeded onto a 96-well plate (5000 cells/well). The cells were subjected to H/R, followed by cell proliferation assays at 0, 24, and 48 hours. No significant difference in cell proliferation was observed between the treatment groups at 0 hours. However, the C.siRNA+H/R group showed significantly increased cell proliferation at both 24 hours (697.3±11.27) and 48 hours (888.9±25.86) compared with C.siRNA alone (251.1±3.84 and 408±11.12, respectively). This H/R-mediated increase in cell proliferation was inhibited in the Peli1.siRNA- treated group at both 24 hours (413.1±21.69) and 48 hours (506.1±29.71), indicating that Peli1 plays an important role in cell proliferation (Figure 3J).

An in vitro scratch assay was performed to assess the migration potential of HUVECs subjected to H/R. In the absence of Peli1 (Figure 3K), H/R-mediated wound closure was found to be significantly affected at 3, 6, 12, 24, and 36 hours after injury. Substantially more cell migration was observed in the C.siRNA+H/R group compared with the C.siRNA group at 3 hours (13.34±1.01% versus 7.06±1.6%), 6 hours (24.68±1.55% versus 11.19±2.0%), 12 hours (39.74±1.91% versus 17.22±1.54%), 24 hours (71.68±2.04% versus 23.87±1.27%), and 36 hours (90.75±2.07% versus 54.05±2.09%). However, the H/R-mediated increase in cell

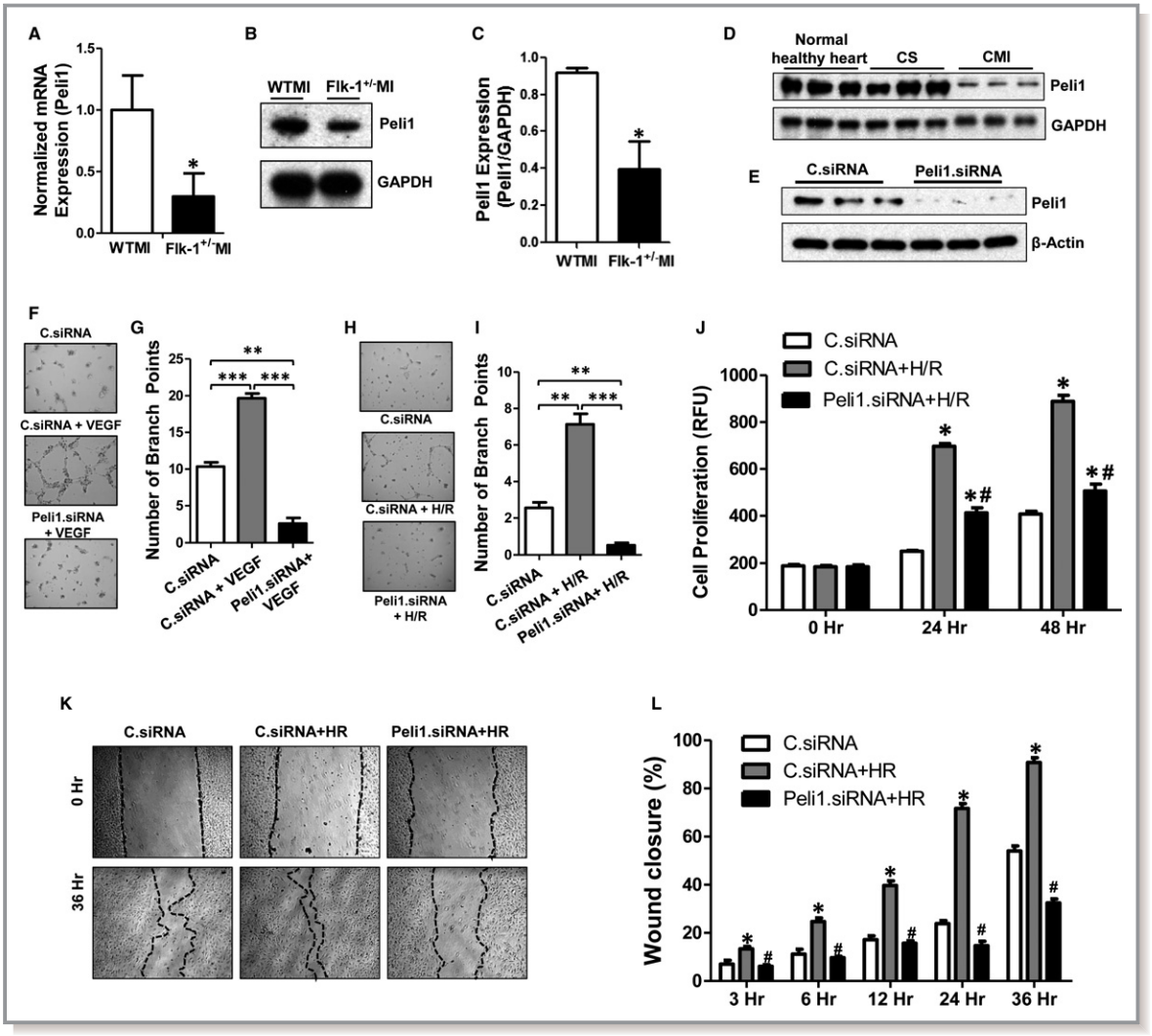

Figure 3. Peli1 is reduced in Flk-$1^{+/-}$ MI mice. A, The bar graph shows the mRNA expression of Peli1 in WTMI and Flk-$1^{+/-}$MI mice (n=5-7/group) (8 hours after surgery). B, Western blot analysis of Peli1 and GAPDH protein in the WTMI and Flk-$1^{+/-}$MI groups (4 days after surgery). C, The bar graphs represent Peli1 levels normalized to GAPDH. The Flk-$1^{+/-}$MI group showed reduced levels of Peli1 compared with WTMI (n=3/group) (*P<0.05). D, Representative Western blot picture showing the expression of Peli1 in normal healthy and control hearts subjected to sham and after MI procedure (4 days after surgery) (n=3/group). E, Representative Western blot showing the expression of Peli1 in C.siRNA and Peli1.siRNA-treated HUVECs (n=3/group). F through L, Peli1 knockdown inhibits tube formation, cell proliferation, and migration. F and G, HUVECs were treated with either C.SiRNA or Peli1.siRNA, followed by VEGF treatment, and subjected to the tube-formation assay. G, Bar graph representing the total number of branch points in different treatment groups. The C.siRNA+VEGF treatment group showed an increased number of branch points compared with the C.siRNA-alone group, whereas the Peli1.siRNA+VEGF treatment group showed a decreased number of branch points compared with both the C.siRNA-alone and C.siRNA+VEGF treatment groups (n=3/group) (**P<0.01, ***P<0.001). H and I, HUVECs treated with either C.siRNA or Peli1.siRNA followed by H/R treatment and subjected to the tube-formation assay. I, Bar graph representing the total number of branch points in different treatment groups (n=3/group) (**P<0.01, ***P<0.001). The C.siRNA+H/R treatment group showed an increased number of branch points compared with C.siRNA, whereas the Peli1.siRNA+H/R treatment group showed a decreased number of branch points compared with C.siRNA+H/R. J, Bar graph representing the cell proliferation at 0, 24, and 48 hours after seeding (n=6/group). K, Representative pictures of wound closure in different treatment groups at 0 and 36 hours after treatment. L, Bar graph representing the percentage cell-wound closure at 3, 6, 12, 24, and 36 hours after injury in different treatment groups. The C.siRNA+H/R group showed increased cell proliferation and wound closure compared with the C.siRNA group, whereas the Peli1.siRNA+H/R group showed decreased cell proliferation and wound closure compared with the C.siRNA+H/R group. Values are mean±SEM. *P<0.05 compared with the C.siRNA group; #P<0.05 compared with the C.siRNA+H/R group. C.siRNA indicates control siRNA-treated group; CMI, control MI; CS, control sham; Flk-$1^{+/-}$MI, Flk-$1^{+/-}$ mice subjected to MI; GAPDH, glyceraldehyde 3-phosphate dehydrogenase; H/R, hypoxia/reoxygenation; HUVEC, human umbilical vein endothelial cells; MI, myocardial infarction; Peli1, Pellino-1; Peli1.siRNA, Peli1 siRNA treated group; VEGF, vascular endothelial growth factor; WT, wild-type; WTMI, WT mice subjected to MI.

migration/wound closure was inhibited by Peli1.siRNA at 3 hours (6.14±0.67%), 6 hours (9.73±0.60%), 12 hours (15.72±1.1%), 24 hours (14.74±1.80%), and 36 hours (32.45±1.66%) (Figure 3L).

Efficient In Vivo Peli1 Gene Expression in the Ischemic Myocardium of CD1 (WT) Mice Following Adenoviral Injection

Immunohistochemistry (Figure S2) and Western blot analysis (Figure 4A) were performed 4 days after the administration of Ad-Peli1 to detect the expression of Peli1 in Ad-LacZ- and Ad-Peli1-injected hearts without MI (n=3/group). Both of the techniques increased Peli1 expression in mice treated with Ad-Peli1, compared with the Ad-LacZ-treated group. Additionally, Western blot analysis of hearts treated with Ad-LacZ or Ad-Peli1 and subjected to MI showed that Peli1 expression was more robust in the Ad-Peli1 group (9.9-fold) than in the Ad-LacZ group (Figure 4B and 4C).

Peli1 Promotes Akt/MK2/p-IκBα/eNOS Signaling and β-Catenin Translocation During MI

Western blot analysis was performed to analyze the downstream signaling molecules and gap junction proteins involved in the Peli1-mediated rescue of the infarcted myocardium 24 hours and 4 days after the induction of MI. The expressions of Akt, MK2, eNOS, IκBα, and β-catenin proteins were determined. The Western blot analysis showed increased

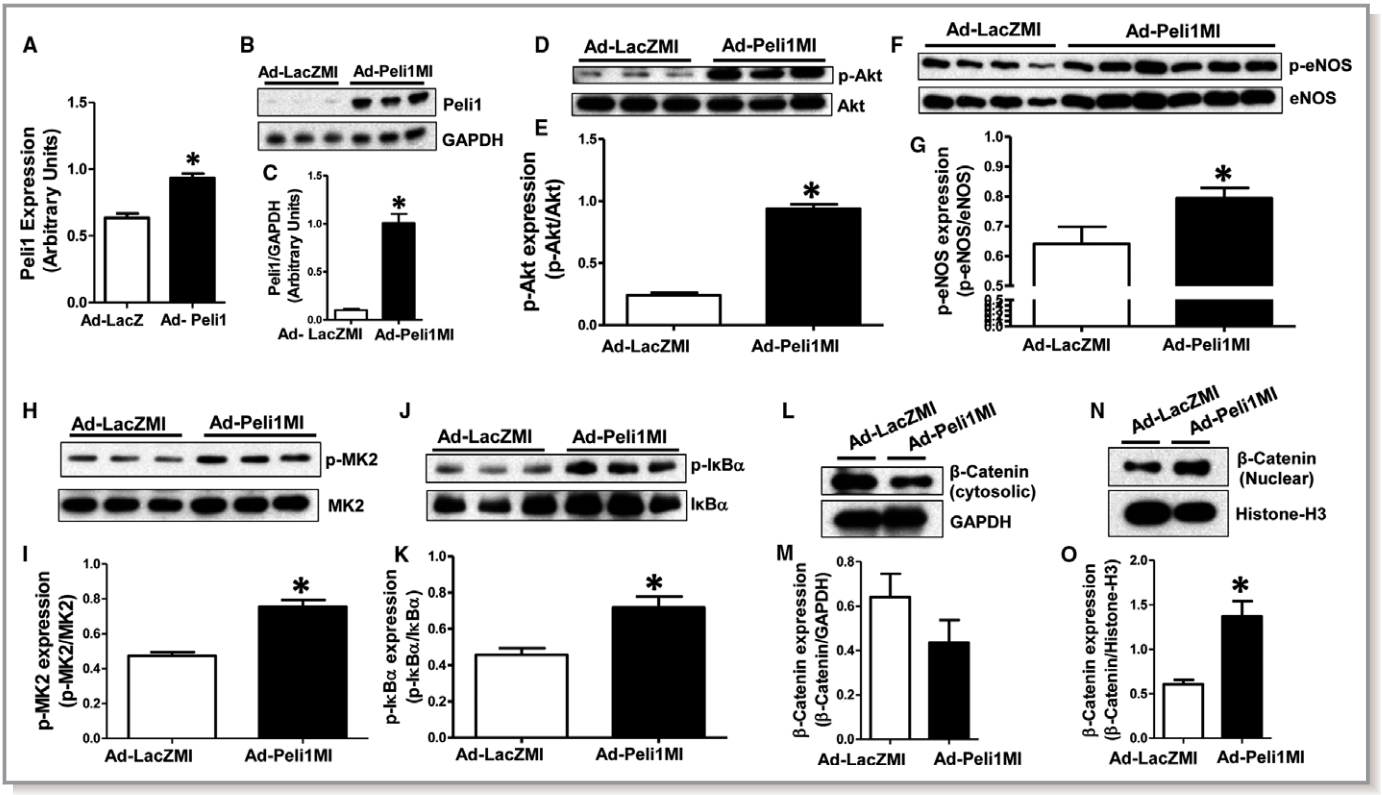

Figure 4. Transfection efficiency. A, Bar graph shows the expression of Ad-LacZ and Ad-Peli1 in control heart tissues by Western blot analysis 4 days after injection (n=3/group). B, Representative Western blot analysis of Peli1expression, 4 days after MI in CD1 in mice. C, Bar graphs represent Peli1 expression normalized to GAPDH (n=3/group). Peli1 overexpression increased the phosphorylation of Akt, eNOS, MK2, and IκBα after MI. D, Western blot analysis of p-Akt and Akt (24 hours after MI). E, Bar graphs represent p-Akt levels normalized to total Akt levels (n=3/group). F, Western blot analysis of p-eNOS and eNOS (24 hours after MI). G, Bar graphs represent p-eNOS levels normalized to total p-eNOS levels (n=4-6/group). H, Western blot analysis of p-MK2 and MK2 (24 hours after MI). I, The bar graphs represent p-MK2 levels normalized to total MK2 levels (n=3/group). J, Western blot analysis of p-IκBα and IκBα (24 hours after MI). K, Bar graphs represent p-IκBα levels normalized to total IκBα levels (n=3/group). L through O, Western blot analyses of the β-catenin expression in both cytosolic (L) and nuclear (N) fraction, 24 hours after MI. M, Bar graphs represent cytosolic β-catenin levels normalized to GAPDH levels (n=5-7/group). O, Bar graphs represent β-catenin levels normalized to histone H3 levels. The Ad-Peli1MI group showed reduced levels of p-Akt, p-eNOS, p-MK2, p-IκBα, and β-catenin translocation compared with the Ad-LacZMI group. Values are mean±SEM. **P*<0.05 compared with the Ad-LacZMI group. Ad-LacZ indicates adenoviral vector encoding LacZ; Ad-LacZMI, CD1 mice subjected to MI followed by Ad-LacZ gene injection; Ad-Peli1, adenoviral vector encoding Peli1; Ad-Peli1MI, CD1 mice subjected to MI followed by Ad-Peli1 gene injection; MI, myocardial infarction.

p-Akt expression in the Ad-Peli1MI group (0.94±0.03) compared with the Ad-LacZMI group (0.24±0.02) (Figure 4D and 4E). Phosphorylation of MK2 was increased in the Ad-Peli1MI group (0.75±0.04) compared with the Ad-LacZMI group (0.47±0.02) (Figure 4H and 4I). The expressions of p-IκBα and p-eNOS were also increased in Ad-Peli1MI mice (0.72±0.06 and 0.79±0.03, respectively) compared with Ad-LacZMI mice (0.46±0.04 and 0.64±0.06, respectively) (Figure 4F, 4G, 4J, and 4K).

Activation of PI3K/Akt signaling was observed in the experiment, as evidenced by increased phosphorylation of Akt and eNOS in Peli1-treated hearts, resulting in the phosphorylation and inactivation of glycogen synthase kinase -3β and accumulation of β-catenin in the cytosol and translocation of the latter to the nucleus. Increased nuclear translocation of β-catenin was observed in the Ad-Peli1MI group compared with Ad-LacZMI mice (1.37±0.17 versus 0.61±0.05) (Figure 4N and 4O). However, no difference in the cytosolic β-catenin level was observed between the Ad-LacZMI and Ad-Peli1MI groups (Figure 4L and 4M).

Peli1 Promotes Cx43 Expression During MI

Immunofluorescent staining of gap junction protein (Cx43) was performed 4 days after MI. Expression of the Cx43 protein was higher in the Ad-Peli1MI group than in the Ad-LacZMI group. The expression intensity of Cx43 in the Ad-Peli1 group was similar to the expression pattern in the Ad-LacZS and Ad-Peli1S mice. The lower intensity of the fluorescent signal detected in the Ad-LacZMI group is indicative of the negative impact of MI (Figure 5A).

Peli1 Preserves the Infarcted Myocardium Through Increased Capillary and Arteriolar Densities

To assess the efficacy of Peli1 treatment in rescuing the infarcted myocardium, we analyzed the numbers of capillaries and arterioles in LV myocardial tissue samples by staining for $CD31^+$ and α-smooth muscle actin–positive cells, respectively. Capillary counts in heart tissue samples

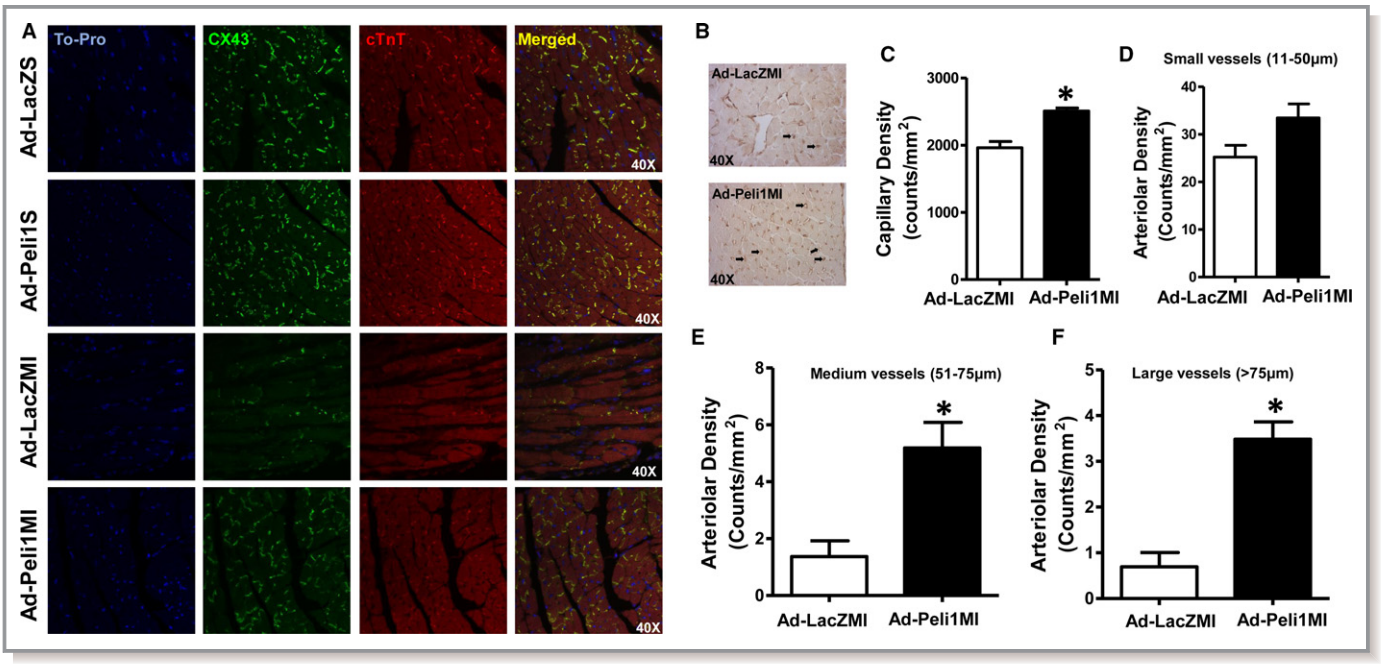

Figure 5. Peli1 overexpression increases Cx43 expression and vessel density. A, Representative confocal images showing the Cx43-positive (green) gap-junctional connections between adjacent cardiomyocytes (red) in the infarct border zone 4 days after the induction of MI in CD1 mice. Nuclei were stained with TO-PRO-3 Iodide (blue). Cx43 levels were similar between the Ad-LacZS and Ad-Peli1S groups. The Ad-LacZMI group showed reduced Cx43 levels compared with both the Ad-LacZS and Ad-Peli1S groups. However, the Ad-Peli1MI group showed increased Cx43 compared with the Ad-LacZMI group (n=5/group). B through F, Measurement of vessel density in mice treated with Ad-LacZ and Ad-Peil1 after the induction of MI in CD1 mice. B, Representative images of CD31 staining for capillary densities, 7 days after MI. Arrows indicate capillaries. C, Bar graph represents the quantitative analysis of capillary density in counts/mm^2. The Ad-Peli1MI treatment group showed an increased capillary density compared with Ad-LacZMI (n=5/group). D through F, Bar graphs represent quantitative analysis of small, medium, and large-sized arteriole densities in counts/mm^2 (30 days after MI). The density of arterioles was increased in the Ad-Peli1MI group compared with Ad-LacZMI. Values are mean SEM, (n=6/group), *P<0.05 compared with the Ad-LacZMI group. Ad-LacZ indicates adenoviral vector encoding LacZ; Ad-LacZMI, CD1 mice subjected to MI followed by Ad-LacZ gene injection; Ad-LacZS, CD1 mice subjected to sham surgery followed by Ad-LacZ gene injection; Ad-Peli1, adenoviral vector encoding Peli1; Ad-Peli1MI, CD1 mice subjected to MI followed by Ad-Peli1 gene injection; Ad-Peli1S, CD1 mice subjected to sham surgery followed by Ad-Peli1 gene injection; Cx43, connexion 43; MI, myocardial infarction; S, Sham.

collected 4 days after surgery were higher in the Ad-Peli1MI group (2508±45.08 counts/mm^2) than in the Ad-LacZMI group (1962±92.99 counts/mm^2), as shown in Figure 5B and 5C.

Staining for α-smooth muscle actin performed 30 days after the induction of MI was positive for arterioles in the ischemic myocardium of both the Ad-LacZ– and Ad-Peli1–treated groups. Representative pictures of small, medium, and large arterioles are shown in Figure S1. Overall counts revealed a greater number of arterioles in the Ad-Peli1MI group compared with the Ad-LacZMI group. More specifically, medium- (5.2±0.9 versus 1.4±0.6 counts/mm^2) and large-sized arterioles (3.5±0.4 versus 0.7±0.3 counts/mm^2) were significantly greater in number in the Ad-Peli1MI group compared with the Ad-LacZMI group. A similar trend was found for small-sized arterioles (33.4±3 versus 25.2±2.5 counts/mm^2 for the Ad-Peli1MI and Ad-LacZMI groups, respectively), but this difference did not reach statistical significance (Figure 5D through 5F).

Peli1 Salvages the Infarcted Myocardium by Reducing Fibrosis and Preserving Cardiac Function

We evaluated the change in cardiac function attributed to Peli1 through echocardiography analysis. The overall status of heart function, as assessed through EF and FS, indicated the physiological status of the heart tissue. No significant difference in EF was observed between the Ad-LacZS and Ad-Peli1S groups, indicating a normal physiological heart status in these groups. However, mice in the Ad-LacZMI group demonstrated a significant reduction in EF compared with Ad-LacZS (32.96±0.98% versus 69.14±1.60%), indicating deterioration of cardiac function associated with MI. Similarly, animals in the Ad-Peli1MI group demonstrated a significant reduction in EF compared with the Ad-Peli1S group (48.49±0.75% versus 66.82±1.72%). However, EF was substantially increased in the Ad-Peli1MI group (48.49±0.75%) compared with Ad-LacZMI (32.96±0.98%), which indicates an acquired cardioprotective effect associated with Peli1 treatment (Figure 6A). Similar findings were observed for FS; compared with the Ad-LacZMI group, Ad-Peli1MI mice showed improved cardiac function (16±0.51% versus 24.54±0.49%) (Figure 6B). An abnormal distribution of collagen in the myocardium is a hallmark feature of myocardial fibrosis. Qualitative analysis by PicroSirus Red staining showed extensive collagen deposition in the Ad-LacZMI group compared with Ad-Peli1MI mice (Figure 6C). Quantitative analysis similarly showed that the fibrotic area of mice in the Ad-Peli1MI group (16.67±1.05%) was significantly reduced compared with that in the Ad-LacZMI group (29.42±2.05%), as shown in Figure 6D.

Ad-Peli1 Gene Therapy Rescues the Ischemic Myocardium in Flk-1$^{+/-}$ Mice

Rescue experiments were performed to determine whether Peli1 is involved in the loss of cardiac function in Flk-1$^{+/-}$ mice subjected to MI and whether treatment with Peli1 using an adenoviral-mediated delivery system could recover heart function in vivo. Flk-1$^{+/-}$ mice that underwent MI were injected with Ad-Peli1 or Ad-LacZ around the ischemic area (risk area). Western blot analysis revealed increased Peli1 expression in Flk-1$^{+/-}$MI+Ad-Peli1 compared with the Flk-1$^{+/-}$MI+Ad-LacZ group (Figure 7A). This was followed by the immunohistochemical analysis of α-smooth muscle actin staining for arteriolar density in Flk-1$^{+/-}$MI mice that underwent Ad-LacZ or Ad-Peli1 treatment. Animals in the Flk-1$^{+/-}$MI+Ad-Peli1 group (28.46±2.0 counts/mm^2) had an increased arteriolar density (smaller arterioles, 11-50 μm) compared with Flk-1$^{+/-}$MI+Ad-LacZ mice (20.07±1.2 counts/mm^2), indicating that Peli1 has a rescue effect on the ischemic myocardium (Figure 7B). However, no statistical differences were observed between the groups in the densities of medium- or large-sized arterioles (Figure 7C and 7D) 30 days post-MI.

Left ventricular function was assessed in Flk-1$^{+/-}$ mice after MI and subsequent injection with either Ad-LacZ or Ad-Peli1 (n=9-11/group) by measuring the LV internal diameter in both systole (LVIDs) and diastole (LVIDd) (Figure 7E and 7F). The ventricles of Flk-1$^{+/-}$MI mice treated with Ad-Peli1 rescue therapy were significantly less dilated in both systole (LVIDs, 4.18±0.16 mm) and diastole (LVIDd, 5.42±0.17 mm) compared with knockdown mice (Flk-1$^{+/-}$) that underwent Ad-LacZ injections following MI (LVIDs, 5.39±0.22 mm; LVIDd, 6.08±0.26 mm) (n=9-11/group). LV end-diastolic volume and LV end-systolic volume were also assessed (Figure 7G and 7H). The LV end-systolic volume was significantly reduced in the Flk-1$^{+/-}$+Ad-Peli1MI group compared with the Flk-1$^{+/-}$+Ad-LacZMI group (79.73±7.62 μL versus 143.5±15 μL) (n=9-11/group). The LV end-diastolic volume was also reduced in the Flk-1$^{+/-}$MI+Ad-Peli1 group compared with Flk-1$^{+/-}$MI+Ad-LacZ, but the difference was not significant (144.5±11.13 μL versus 189.5±20.15 μL) (n=9-11/group). Mice in the Flk-1$^{+/-}$MI+Ad-Peli1 group had significantly improved EF compared with Flk-1$^{+/-}$MI+Ad-LacZ mice (45.36±1.46% versus 24.15±0.87%) (n=9-11/group) (Figure 7I). Contractility of the heart, as measured by FS, was significantly improved in the Flk-1$^{+/-}$MI+Ad-Peli1 group compared with the Flk-1$^{+/-}$+Ad-LacZ group (22.87±0.86% versus 11.36±0.44%) (n=9-11/group) (Figure 7J). Interestingly, we found no difference in the EF (45.36±1.46% versus 48.49±0.75%) or FS (22.87±0.86% versus 24.54±0.5%) between Flk-1$^{+/-}$MI+Ad-Peli1 and Ad-Peli1MI groups (n=10-11/group) (Figure 7K and 7L). However, when these measurements (EF and FS) were compared with the Ad-LacZMI group (EF, 29.83±1.34%; FS,

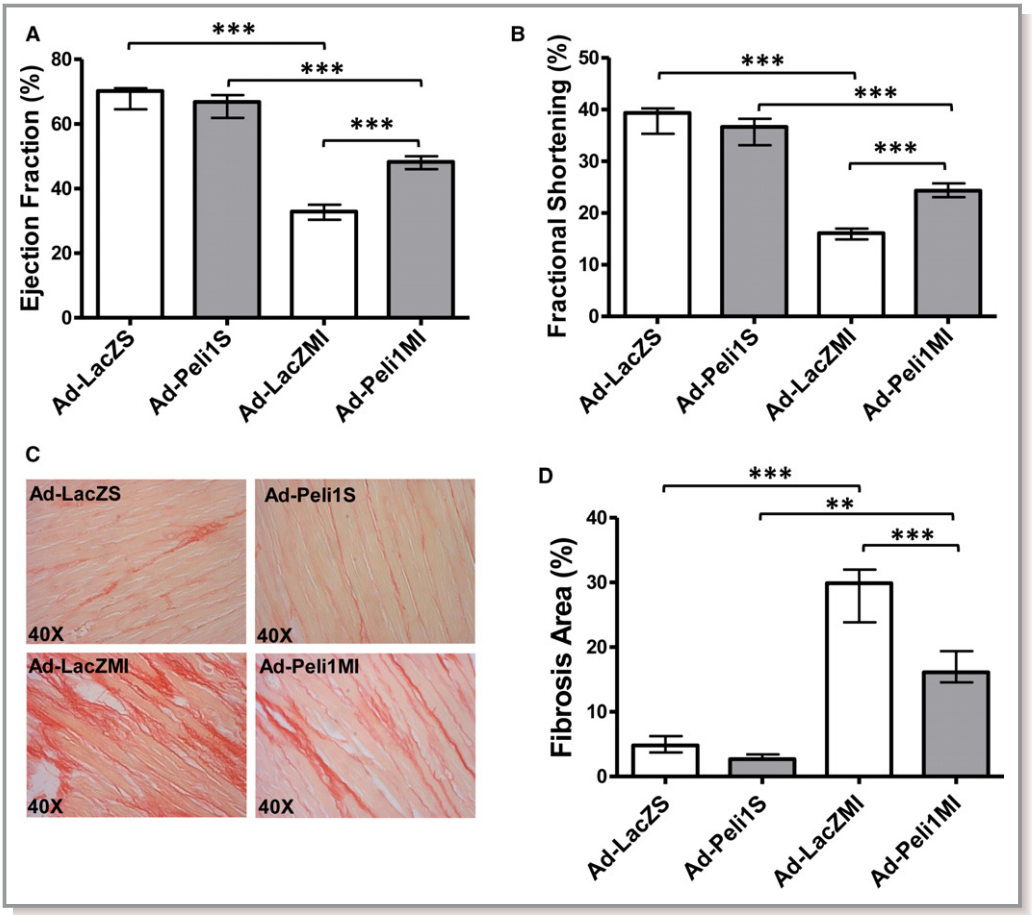

Figure 6. Echocardiographic and fibrosis measurements 30 days after MI in CD1 mice treated with Ad-LacZ or Ad-Peli1. A and B, Measurement of cardiac function, as shown by echocardiographic analysis. The bar graph represents (A) EF and (B) FS measurements. Measurements of cardiac function showed that both EF and FS were increased in the Ad-Peli1MI group compared with Ad-LacZMI. There was no difference between the sham groups in either EF or FS (n=10-12/group). Values in the bar graphs represents median and IQR, (***P<0.001). C, Representative pictures of PicroSirus Red–stained heart sections in both the Ad-LacZMI and Ad-Peli1MI groups. D, Quantitative analysis of myocardial fibrosis. The Ad-Peli1MI treatment group showed decreased myocardial fibrosis compared with Ad-LacZMI (n=5-8/group). Values in the bar graphs represents median and IQR, (**P<0.01, ***P<0.001). Ad-LacZ indicates adenoviral vector encoding LacZ; Ad-LacZMI, CD1 mice subjected to MI followed by Ad-LacZ gene injection; Ad-LacZS, CD1 mice subjected to sham surgery followed by Ad-LacZ gene injection; Ad-Peli1, adenoviral vector encoding Peli1; Ad-Peli1MI, CD1 mice subjected to MI followed by Ad-Peli1 gene injection; Ad-Peli1S, CD1 mice subjected to sham surgery followed by Ad-Peli1 gene injection; EF, ejection fraction; FS, fractional shortening; IQR, interquartile range; MI, myocardial infarction; S, Sham.

14.38±0.67%) (Figure 7K and 7L), they were found to be significantly improved. No difference in EF and FS was found between CMI and Ad-LacZMI groups. Myocardial fibrosis was also attenuated in the Flk-$1^{+/-}$MI+Ad-Peli1 group compared with the Flk-$1^{+/-}$MI+Ad-LacZ mice (7±0.4% versus 14±0.4%). These data indicate substantial treatment potential for Peli1-mediated promotion of cardiac repair in Flk-$1^{+/-}$ mice following MI (Figure 7M and 7N).

Taken together, these data convincingly demonstrate that Ad-Peli1 treatment preserves cardiac function in the myocardium of Flk-$1^{+/-}$ mice by reducing ischemic loss of vessel density and myocardial fibrosis. The results indicate that gene therapy with Ad-Peli1 is strongly correlated with improved cardiac function, as assessed by echocardiogram and cardiac remodeling by myocardial fibrosis.

Discussion

In this study we have shown that Peli1 is a critical factor in VEGF signaling. The reduction of Peli1 expression in Flk-$1^{+/-}$ mice at the baseline and after MI shows that Peli1 functions as a downstream molecule in VEGF/Flk-1 signaling and plays an important role in cardiac repair. In addition, we have also shown that the administration of Peli1 via an adenoviral

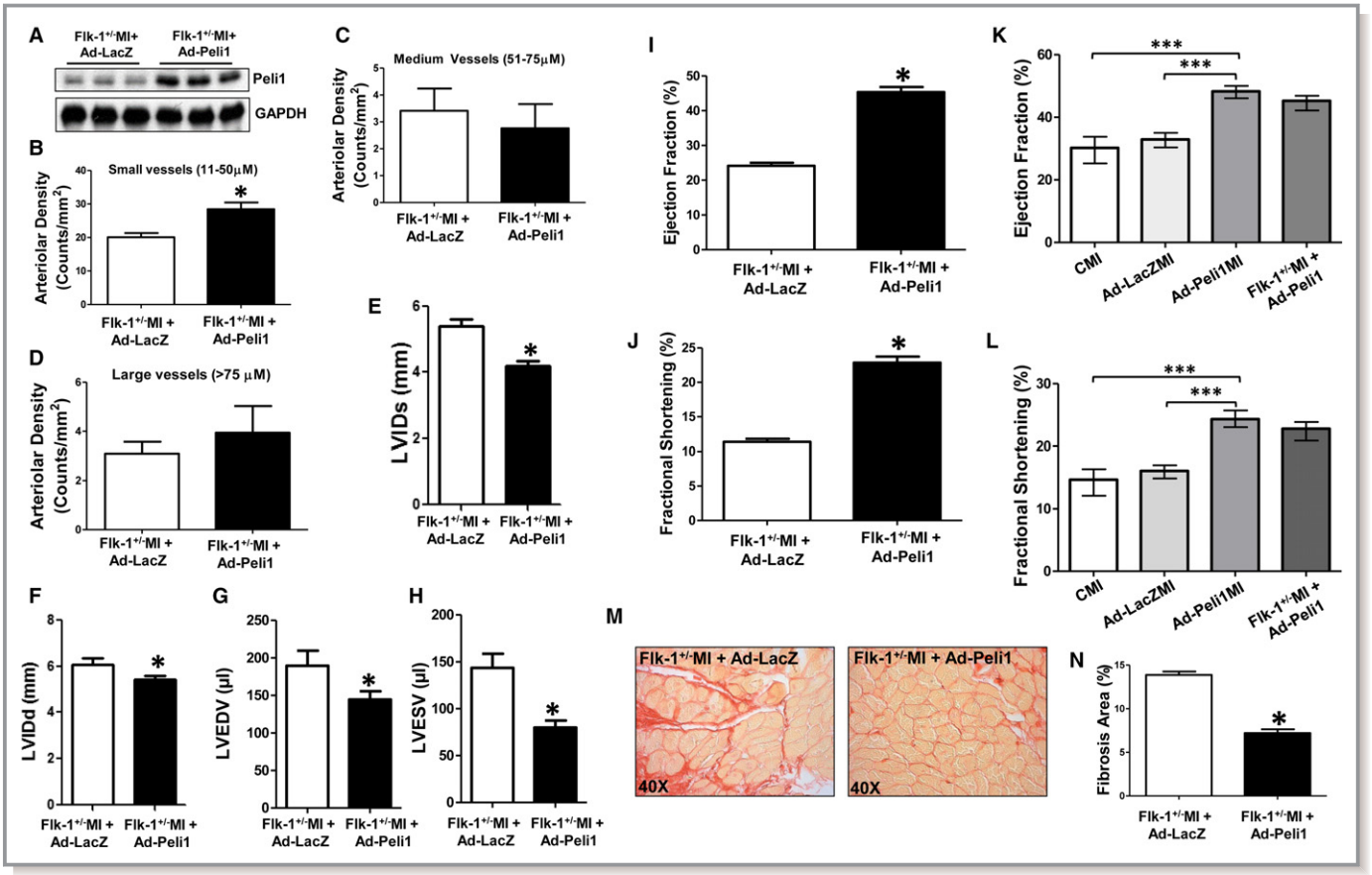

Figure 7. Ad-Peli1 gene therapy administered to Flk-1$^{+/-}$MI mice results in increased vessel densities and cardiac function along with decreased myocardial fibrosis. A, Western blot analysis of Peli1 concentration in Flk-1$^{+/-}$MI+Ad-LacZ and Flk-1$^{+/-}$MI+Ad-Peli1 groups (n=3/group). B through D, The bar graph shows the quantitative analysis of (B) small, (C) medium, and (D) large-sized arterioles in counts/mm^2. There was a significant increase in small vessels in the Flk-1$^{+/-}$MI+Ad-Peli1 group compared with Flk-1$^{+/-}$MI+Ad-LacZ. There were no significant differences in the densities of medium or large vessels between the 2 groups, although there was a trend for an increased density of large vessels in the Flk-1$^{+/-}$MI+Ad-Peli1 group. Values are mean±SEM (n=5/group). *P<0.05 compared with the Flk-1$^{+/-}$MI+Ad-LacZ group. E through J, Cardiac function measured 30 days after MI by echocardiography. E, Left ventricle internal diameter during systole. F, Left ventricle internal diameter during diastole. In both systole and diastole, a significant reduction in internal vessel diameter was observed in Flk-1$^{+/-}$MI+Ad-Peli1 mice compared with Flk-1$^{+/-}$MI+Ad-LacZ mice, indicating a less-dilated left ventricle. G, Left ventricle end-diastolic volume. H, Left ventricle end-systolic volume. A reduction in left ventricle end-diastolic and end-systolic volumes was observed in the Flk-1$^{+/-}$MI+Ad-Peli1, indicating better EF compared with Flk-1$^{+/-}$MI+Ad-LacZ. I through L, Bar graphs represent the EF and FS measurements. Measurements of cardiac function showed that both (I) EF and (J) FS were increased in the Flk-1$^{+/-}$MI+Ad-Peli1 treatment group compared with the Flk-1$^{+/-}$MI+Ad-LacZ group. Values are mean±SEM (n=9-11/group). *P<0.05, Flk-1$^{+/-}$MI+Ad-LacZ group compared with Flk-1$^{+/-}$MI+Ad-Peli1 group. K, EF of CMI, Ad-LacZMI, Ad-Peli1MI, and Flk-1$^{+/-}$MI+Ad-Peli1 groups (n=10-11/group). L, Fractional shortening of CMI, Ad-LacZMI, Ad-Peli1MI, and Flk-1$^{+/-}$MI+Ad-Peli1 groups (n=10-11/group). Ad-Peli1 gene therapy in Flk-1$^{+/-}$MI group (Flk-1$^{+/-}$MI+Ad-Peli1) improved cardiac function to the same degree as Ad-Peli1 gene therapy in WTMI (Ad-Peli1MI) in both EF and FS. These measurements were both improved when compared with the CMI and Ad-LacZMI groups. No statistical difference was observed between the CMI and Ad-LacZMI groups or between the Ad-Peli1MI and Flk-1$^{+/-}$MI+Ad-Peli1 groups in either EF or FS. Values in the bar graphs (K and L) represent median and IQR, (n=10-11/group), (***P<0.001). M and N, Myocardial fibrosis. M, Representative pictures of PicroSirius Red staining. N, Quantitative analysis of myocardial fibrosis (30 days after MI). The Flk-1$^{+/-}$MI+Ad-Peli1 group showed decreased fibrosis compared with Flk-1$^{+/-}$MI+Ad-LacZ. Values are mean±SEM (n=7-11/group). *P<0.05 compared with the Flk-1$^{+/-}$MI+Ad-LacZ group. Ad-LacZMI indicates CD1 mice subjected to MI followed by Ad-LacZ injection; Ad-Peli1MI, CD1 mice subjected to MI followed by Ad-Peli1 injection; CMI, control (CD1) mice subjected to MI, without gene therapy; EF, ejection fraction; Flk-1$^{+/-}$MI+Ad-LacZ, Flk-1$^{+/-}$ mice subjected to MI followed by Ad-LacZ injection; Flk-1$^{+/-}$MI+Ad-Peli1, Flk-1$^{+/-}$ mice subjected to MI followed by Ad-Peli1 injection; FS, fractional shortening; IQR, interquartile range; LVEDV, left ventricular end diastolic volume; LVESV, left ventricular end systolic volume; LVIDd, left ventricular internal diameter at diastole; LVIDs, left ventricular internal diameter at systole; MI, myocardial infarction; NS, not significant; SEM, standard error of the mean; WT, wild type.

vector induces an angiogenic response and improved heart function, and it ameliorates ventricular remodeling in a genetic knockout mouse model (Flk-1$^{+/-}$).

Notably, we observed that inhibition of Flk-1 in a mouse model of MI caused reduced expression of several key signaling molecules and inhibition of Flk-1 phosphorylation,

highlighting the importance of Flk-1 in the angiogenic process (Figure 8A). Given the observed effects of Flk-1 inhibition, the role of Peli1 in angiogenesis is an area of interest. Western blot and PCR analyses (Figure 3A through 3C) showing downregulation of Peli1 in Flk-$1^{+/-}$ mice confirm the connection between Peli1 and the upstream regulator VEGFR2/Flk-1. Additionally, in vitro studies showing that the silencing of Peli1 inhibits VEGF and hypoxia-induced tubulogenesis which indicate that Peli1 plays a significant role in the angiogenic process.

The importance of Peli1 in angiogenesis was authenticated by the results of Ad-Peli1 gene therapy studies. Compared with mice in the nontreated Ad-LacZ group, several signaling factors were upregulated in the Ad-Peli1 therapy group, including p-Akt, p-eNOS, p-MK2, and p-IκBα. In addition, increased expression of Cx43 indicated greater communication between myocardial cells through gap junctions. Decreased myocardial fibrosis suggested reduced cardiac injury and fibrotic scarring. Increased capillary and arteriolar densities demonstrated the formation of new vessels in the presence of Peli1. Improved echocardiographic parameters in Ad-Peli1–treated mice provided evidence of improved myocardial function. Taken together, these results demonstrate that the induction of angiogenesis by Peli1, as observed by increased vessel formation, may be beneficial in patients who have suffered MI (Figure 8B). This is the first study to observe Peli1-mediated salvage of Flk-1 signaling in an MI model and to demonstrate its proangiogenic and cardioprotective properties.

Nuclear factor κ light-chain enhancer of activated B cells controls the transcription of various angiogenic factors and is also involved in cytokine production and cell survival. Evidence indicates that oxidative stress and the production of free radicals secondary to MI lead to the activation of NFκB, which, in turn, induces the expression of genes involved in angiogenesis.[28,29] In a mouse model the administration of pyrrolidine dithiocarbamate, an inhibitor of NFκB, has been shown to block neovascularization, indicating that activation of NFκB is an obligatory component of retinal angiogenesis.[30] Notably, Peli1 has been shown to upregulate levels of NFκB in inflammatory cells. Peli1 interacts with interleukin-1 receptor-associated kinase-4, interleukin-1 receptor-associated kinase, and tumor necrosis factor receptor–associated factor-6 to activate the IKK complex. The IKK complex, in turn, reacts with IκB and leads to the activation of NFκB.[31] In its dephosphorylated state IκB binds to NFκB in the cytoplasm, preventing it from entering the nucleus for transcription. However, when activated, the IKK complex triggers phosphorylation, ubiquitination, and ultimately the degradation of IκB, allowing for the activation of NFκB.[32] In this study we showed increased p-IκBα levels in the Ad-Peli1MI group compared with the Ad-LacZMI group. We observed reductions in p-IκBα and NFκB activity of mice with knockdown of Flk-1 in MI and ischemic preconditioning and in the inhibition of Flk-1 in vitro. We also observed increases in p-IκBα and NFκB in Peli1-treated mice. Upregulation of NFκB implicates Peli1 in the cardioprotective process, and the increase in p-IκBα offers insight into the mechanism through which Peli1 may work.

The observed upregulation of p-MK2 in our study establishes that Peli1 can induce angiogenesis. Phosphorylation of MK2 significantly increases the activation of NFκB.[8] In microglial cells, MK2 activity is inhibited by tumor necrosis factor receptor–associated factor-3. Peli1 activates inhibitor of apoptosis-2, which in turn facilitates the degradation of tumor necrosis factor receptor–associated factor-3 and liberates MK2 to activate NFκB.[33] Accordingly, a deficiency of Peli1 in microglial cells has been shown to be associated with reduced activation of IAP2 and MK2.[14] In this study we established that Peli1 could also upregulate MK2 activation in heart tissue to stimulate angiogenesis. Upregulation of MK2 subsequently led to further expression of NFκB, providing support for the hypothesis that Peli1 increases activation of NFκB to promote cardiac repair. This finding not only provides evidence for the potential benefits of Peli1 but also offers further insight into its mechanism of action.

Phosphatidylinositol 3-kinase (PI3K) and its downstream survival targets play important roles in signaling pathways involved in cardioprotection.[34] Some important downstream targets of PI3K include the phosphorylation of Akt and glycogen synthase kinase-3β. Increased levels of p-glycogen synthase kinase-3β stabilize and accumulate β-catenin in the cytosol, which is followed by translocation into the nucleus.[35] β-Catenin is known to be a strong mediator of angiogenesis.[36] Interestingly, in our study Peli1 gene therapy was found to trigger greater activation and nuclear translocation of β-catenin in the Ad-Peli1MI group than in the Ad-LacZMI group. Previously, we highlighted the importance of PC-mediated upregulation of β-catenin expression in angiogenic responses and cardioprotection[36]; silencing of β-catenin was found to abolish PC-mediated increases in proangiogenic effects and heart health.[36] Therefore, activation of β-catenin by Peli1 could represent a promising strategy for improving cardiac function after MI. Increases in the expression of p-Akt and p-eNOS also strengthen the case for Peli1 as a proangiogenic molecule. In response to VEGF stimulation, Akt aids in endothelial cell migration and proliferation by inducing capillary formation, mobilizing endothelial cell progenitors, and increasing the production of eNOS.[37] In addition, Akt inhibits the production of caspase-9, a molecule that favors apoptosis.[38] Similarly, eNOS produces nitric oxide in endothelial cells, which increases vasodilation, vascular permeability, endothelial cell migration, and blood vessel maturation. A previous study showed that vildagliptin, a dipeptidyl

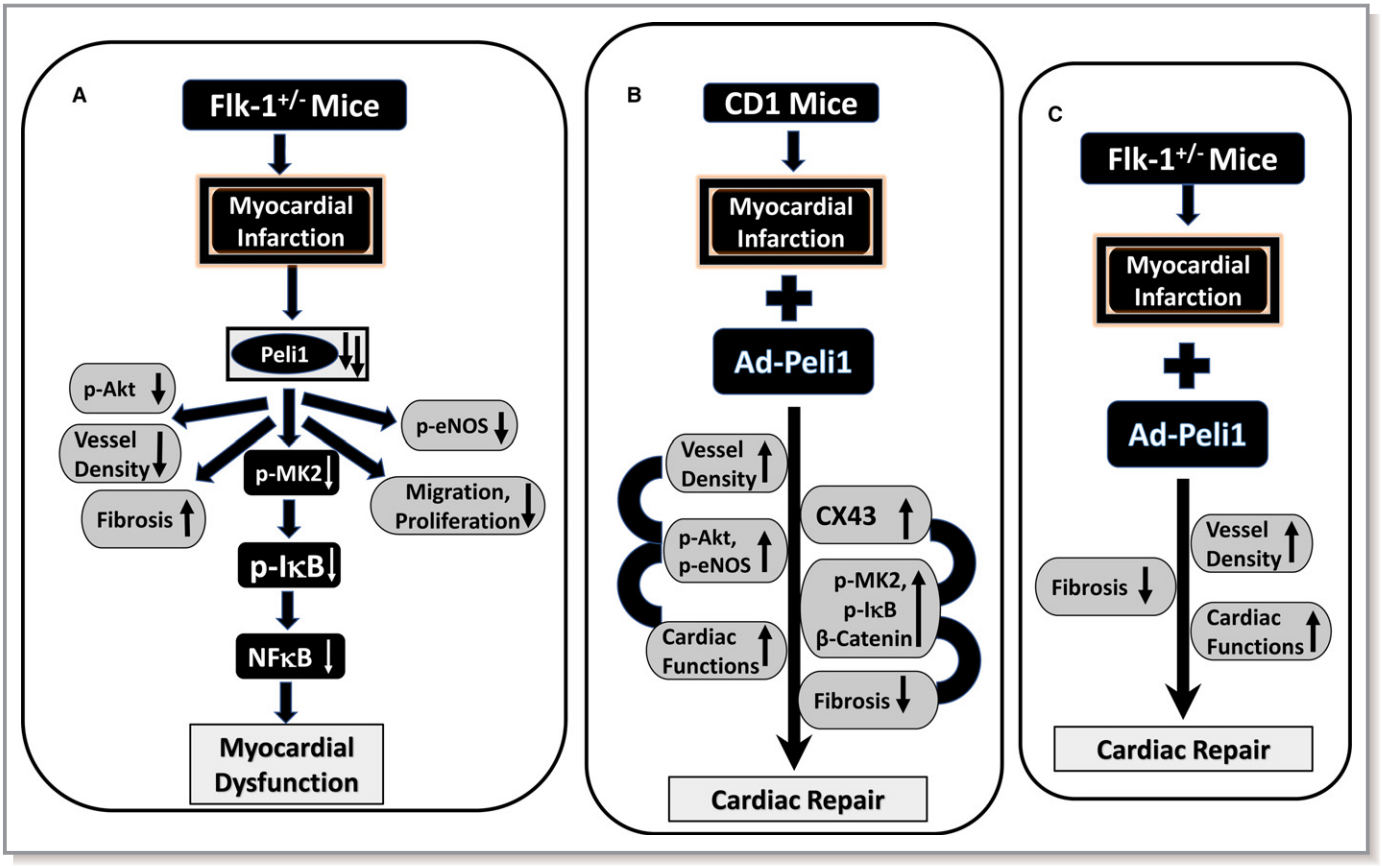

Figure 8. Molecular mechanism of VEGF/FLK-1/Peli-1 molecular signaling in the infarcted myocardium. A, Flow diagram showing how disruption of Flk-1 signaling leads to myocardial dysfunction: Flk-1 KO (Flk-$1^{+/-}$) mice subjected to MI reduced Peli1 expression, followed by reduced phosphorylation of MK2, Akt, eNOS, and IκBα, reduced cell proliferation, migration, and vessel density, and to increased fibrosis. B, Ad-Peli gene therapy improves cardiac function and ameliorates ventricular remodeling after MI. Peli1 gene therapy triggered increased phosphorylation of Akt, eNOS, MK2, and IκBα, increased Cx43 expression, and reduced fibrosis. C, Ad-Peli1 gene therapy rescues Flk-1 KO mice after MI. Ad-Peli1 gene therapy leads to increased vessel density and cardiac function and to reduced fibrosis in Flk-1KO mice subjected to MI. KO indicates knockout; MI, myocardial infarction.

peptidase-4 inhibitor, stimulates ischemia-induced revascularization in WT mice but not in those that are deficient in eNOS.[39] In another study, the inhibition of eNOS or overexpression of dominant-negative Akt was observed to stunt VEGF-induced endothelial cell migration, whereas overexpression of active Akt promoted cell migration.[40]

This study found significant increases in both Akt and eNOS activity in Ad-Peli1MI mice compared with Ad-LacZMI mice, indicating that Peli1 is involved in the induction of eNOS and that the potential mechanism by which it acts is through the activation of Akt. The increase in eNOS ultimately protects the heart from further damage.

Cx43 is a component of gap junctions that provides a means of cell-to-cell communication and aids in the electrical activation of heart tissue. A previous study found that VEGF upregulated expression of Cx43 and that inhibition of VEGF downregulated Cx43 expression.[41] Another study revealed that in cardiac organoids, or engineered simplified heart chambers, VEGF upregulated Cx43 and enhanced cardiac function.[42] A third study established that Cx43 overexpression in mesenchymal stem cells promoted angiogenesis in the infarcted myocardium, whereas knockdown of Cx43 by siRNA in MI reduced angiogenesis.[43] In this study we observed significant overexpression of Cx43 in Ad-Peli1MI mice compared with Ad-LacZMI mice. Because increased intracellular communication between cardiomyocytes allows for more synchronized and efficient cardiac healing, Peli1 therefore has the potential to improve networking between/among heart cells and allow for better recovery.

We observed a significant increase in arteriogenesis 30 days following MI in Ad-Peli1 mice compared with Ad-LacZMI mice. Thirty days after the induction of MI, treatment with Ad-Peli1 clearly demonstrated increases in arterioles with diameters ranging from 51 to 75 μm (medium vessels) and >75 μm (large vessels). This finding is indicative of enhanced arteriogenesis in the treatment group and can likely be attributed to increased phosphorylation of MK2, Akt, eNOS, and IκBα and increased expression of β-catenin. These molecules contributed to

neovascularization in the Peli1 treatment group, and the increase in vasculature would have subsequently allowed for increased oxygenation and nutrient supply to the damaged heart, hastening recovery. The cardioprotective properties of Peli1 and these molecules are also sufficient to explain the observed reduction in the extent of fibrosis in the Ad-Peli1MI group compared with the Ad-LacZMI group.

Compared with both the WTMI and Ad-LacZMI groups, a significant increase in the cardiac function of Ad-Peli1MI mice was observed. This increase was correlated with enhanced EF, FS, systolic internal diameter, and diastolic internal diameter. MI has been attributed to decreased cardiac function as well as diastolic and systolic dysfunction, most likely because ischemic damage to the myocardium reduces its ability to contract. Increased cardiac function is also related to the observation of reduced fibrosis in Ad-Peli1 mice. The findings of this study can be attributed to increased vessel health and to the cardioprotective effect of Peli1 realized through its influence on the VEGF pathway. Overall, our results demonstrate that Flk-1 plays a significant role in the angiogenic process following ischemic damage. Inhibition of Flk-1 leads to the downregulation of various proangiogenic factors, including Peli1, reduced ability of the heart to undergo neovascularization, and increased damage to the myocardium (Figures 1, 2, and 3A through 3C). Flk-1 provides the body with mechanisms to alleviate injury and protects the heart under ischemic threat. Accordingly, a reduction or inhibition of this critical molecule leads to a decline in the cardioprotective process. The protective effects of Peli1 on the heart under ischemic insult are shown in Figures 3 through 6; administration of Peli1 increases the expression of numerous proangiogenic factors, enhances neovascularization, and ameliorates many of the negative effects of MI. In addition, we have shown that Peli1 overexpression in Flk-$1^{+/-}$ mice (Ad-Peli1 gene therapy) after MI rescues the ischemic myocardium (Figure 8C) from further injury, resulting in improved ventricular function through increased arteriogenesis and reduced cardiac fibrosis (Figure 7). In addition, we recently showed that Peli1 could increase the survivability of ischemic skin-flap tissue in Flk-$1^{+/-}$ mice by increasing blood perfusion and reducing inflammation and necrosis.[11] The connection between the downregulation of Flk-1 and reduced expression of Peli1 suggests that the adverse consequences of reducing Flk-1 may be due to the reduction of Peli1.

In conclusion, we have successfully demonstrated that Peli1 plays a role in VEGF/Flk1 signaling in response to MI. Deletion of Flk1 abruptly suppressed VEGF-mediated signaling, resulting in the inhibition of angiogenesis and decreased heart function due to downregulation of Peli1 expression during MI. However, supplementation of Peli1 revived downstream VEGF signaling in Flk-1 knockout mice, induced angiogenesis, and increased cardiac repair and heart functions. These findings suggest that Peli1 is an important downstream target of VEGF. This innovative approach may prove to be a valuable therapeutic treatment for cardiovascular disease and may improve both the longevity and quality of life of affected patients.

Acknowledgments

We would like to give special thanks to Dr Rajesh Lakshmanan for his help in the preparation of the manuscript and Dr Lulu Rahman for her help in immunohistochemistry.

Sources of Funding

This study was supported by National Institutes of Health grant GM112957 to N Maulik.

Disclosures

None.

References

1. Go AS, Mozaffarian D, Roger VL, Benjamin EJ, Berry JD, Borden WB, Bravata DM, Dai S, Ford ES, Fox CS, Franco S, Fullerton HJ, Gillespie C, Hailpern SM, Heit JA, Howard VJ, Huffman MD, Kissela BM, Kittner SJ, Lackland DT, Lichtman JH, Lisabeth LD, Magid D, Marcus GM, Marelli A, Matchar DB, McGuire DK, Mohler ER, Moy CS, Mussolino ME, Nichol G, Paynter NP, Schreiner PJ, Sorlie PD, Stein J, Turan TN, Virani SS, Wong ND, Woo D, Turner MB. Executive summary: heart disease and stroke statistics—2013 update: a report from the American Heart Association. *Circulation*. 2013;127:143–152.
2. Guo H, Zhou H, Lu J, Qu Y, Yu D, Tong Y. Vascular endothelial growth factor: an attractive target in the treatment of hypoxic/ischemic brain injury. *Neural Regen Res*. 2016;11:174–179.
3. Hoeben A, Landuyt B, Highley MS, Wildiers H, Van Oosterom AT, De Bruijn EA. Vascular endothelial growth factor and angiogenesis. *Pharmacol Rev*. 2004;56:549–580.
4. Samuel SM, Akita Y, Paul D, Thirunavukkarasu M, Zhan L, Sudhakaran PR, Li C, Maulik N. Coadministration of adenoviral vascular endothelial growth factor and angiopoietin-1 enhances vascularization and reduces ventricular remodeling in the infarcted myocardium of type 1 diabetic rats. *Diabetes*. 2010;59:51–60.
5. Stewart DJ, Kutryk MJ, Fitchett D, Freeman M, Camack N, Su Y, Siega AD, Bilodeau L, Burton JR, Proulx G, Radhakrishnan S. VEGF gene therapy fails to improve perfusion of ischemic myocardium in patients with advanced coronary disease: results of the NORTHERN trial. *Mol Ther*. 2009;17:1109–1115.
6. Giacca M, Zacchigna S. VEGF gene therapy: therapeutic angiogenesis in the clinic and beyond. *Gene Ther*. 2012;19:622–629.
7. Kastrup J. Gene therapy and angiogenesis in patients with coronary artery disease. *Expert Rev Cardiovasc Ther*. 2010;8:1127–1138.
8. Ghosh S, Hayden MS. New regulators of NF-κB in inflammation. *Nat Rev Immunol*. 2008;8:837–848.
9. Boengler K, Schulz R, Heusch G. Connexin 43 signalling and cardioprotection. *Heart*. 2006;92:1724–1727.
10. Wang HH, Su CH, Wu YJ, Li JY, Tseng YM, Lin YC, Hsieh CL, Tsai CH, Yeh HI. Reduction of connexin43 in human endothelial progenitor cells impairs the angiogenic potential. *Angiogenesis*. 2013;16:553–560.
11. Rednam CK, Wilson RL, Selvaraju V, Rishi MT, Thirunavukkarasu M, Coca-Soliz V, Lakshmanan R, Palesty JA, McFadden DW, Maulik N. Increased survivability of ischemic skin flap tissue in Flk-$1^{+/-}$ mice by Pellino-1 intervention. *Microcirculation*. 2017;24:e12362.
12. Thirunavukkarasu M, Addya S, Juhasz B, Pant R, Zhan L, Surrey S, Maulik G, Menon VP, Maulik N. Heterozygous disruption of Flk-1 receptor leads to myocardial ischaemia reperfusion injury in mice: application of affymetrix gene chip analysis. *J Cell Mol Med*. 2008;12:1284–1302.

13. Schauvliege R, Janssens S, Beyaert R. Pellino proteins: novel players in TLR and IL-1R signalling. *J Cell Mol Med*. 2007;11:453–461.
14. Xiao Y, Jin J, Chang M, Chang JH, Hu H, Zhou X, Brittain GC, Stansberg C, Torkildsen O, Wang X, Brink R, Cheng X, Sun SC. Peli1 promotes microglia-mediated CNS inflammation by regulating Traf3 degradation. *Nat Med*. 2013;19:595–602.
15. Chang M, Jin W, Sun SC. Peli1 facilitates TRIF-dependent Toll-like receptor signaling and proinflammatory cytokine production. *Nat Immunol*. 2009;10:1089–1095.
16. Sizemore N, Lerner N, Dombrowski N, Sakurai H, Stark GR. Distinct roles of the Iκ B kinase α and β subunits in liberating nuclear factor κB (NF-κB) from IκB and in phosphorylating the p65 subunit of NF-κB. *J Biol Chem*. 2002;277:3863–3869.
17. Madrid LV, Mayo MW, Reuther JY, Baldwin AS Jr. Akt stimulates the transactivation potential of the RelA/p65 subunit of NF-κB through utilization of the IκB kinase and activation of the mitogen-activated protein kinase p38. *J Biol Chem*. 2001;276:18934–18940.
18. Agarwal A, Das K, Lerner N, Sathe S, Cicek M, Casey G, Sizemore N. The Akt/IκB kinase pathway promotes angiogenic/metastatic gene expression in colorectal cancer by activating nuclear factor-κB and β-catenin. *Oncogene*. 2005;24:1021–1031.
19. Goetsch KP, Niesler CU. Optimization of the scratch assay for in vitro skeletal muscle wound healing analysis. *Anal Biochem*. 2011;411:158–160.
20. Liang CC, Park AY, Guan JL. In vitro scratch assay: a convenient and inexpensive method for analysis of cell migration in vitro. *Nat Protoc*. 2007;2:329–333.
21. Adluri RS, Thirunavukkarasu M, Zhan L, Akita Y, Samuel SM, Otani H, Ho YS, Maulik G, Maulik N. Thioredoxin 1 enhances neovascularization and reduces ventricular remodeling during chronic myocardial infarction: a study using thioredoxin 1 transgenic mice. *J Mol Cell Cardiol*. 2011;50:239–247.
22. Miller DL, Van Winkle DM. Ischemic preconditioning limits infarct size following regional ischemia-reperfusion in in situ mouse hearts. *Cardiovasc Res*. 1999;42:680–684.
23. Thirunavukkarasu M, Adluri RS, Juhasz B, Samuel SM, Zhan L, Kaur A, Maulik G, Sanchez JA, Hager J, Maulik N. Novel role of NADPH oxidase in ischemic myocardium: a study with Nox2 knockout mice. *Funct Integr Genomics*. 2012;12:501–514.
24. Wissmann C, Detmar M. Pathways targeting tumor lymphangiogenesis. *Clin Cancer Res*. 2006;12:6865–6868.
25. Holmes K, Roberts OL, Thomas AM, Cross MJ. Vascular endothelial growth factor receptor-2: structure, function, intracellular signalling and therapeutic inhibition. *Cell Signal*. 2007;19:2003–2012.
26. Fulton D, Gratton JP, McCabe TJ, Fontana J, Fujio Y, Walsh K, Franke TF, Papapetropoulos A, Sessa WC. Regulation of endothelium-derived nitric oxide production by the protein kinase Akt. *Nature*. 1999;399:597–601.
27. Jia H, Bagherzadeh A, Bicknell R, Duchen MR, Liu D, Zachary I. Vascular endothelial growth factor (VEGF)-D and VEGF-A differentially regulate KDR-mediated signaling and biological function in vascular endothelial cells. *J Biol Chem*. 2004;279:36148–36157.
28. Ladoux A, Frelin C. Expression of vascular endothelial growth factor by cultured endothelial cells from brain microvessels. *Biochem Biophys Res Commun*. 1993;194:799–803.
29. Stoltz RA, Abraham NG, Laniado-Schwartzman M. The role of NF-κB in the angiogenic response of coronary microvessel endothelial cells. *Proc Natl Acad Sci USA*. 1996;93:2832–2837.
30. Yoshida A, Yoshida S, Ishibashi T, Kuwano M, Inomata H. Suppression of retinal neovascularization by the NF-κB inhibitor pyrrolidine dithiocarbamate in mice. *Invest Ophthalmol Vis Sci*. 1999;40:1624–1629.
31. Jiang Z, Johnson HJ, Nie H, Qin J, Bird TA, Li X. Pellino 1 is required for interleukin-1 (IL-1)-mediated signaling through its interaction with the IL-1 receptor-associated kinase 4 (IRAK4)-IRAK-tumor necrosis factor receptor-associated factor 6 (TRAF6) complex. *J Biol Chem*. 2003;278:10952–10956.
32. Beg AA, Baldwin AS Jr. The I kappa B proteins: multifunctional regulators of Rel/NF-kappa B transcription factors. *Genes Dev*. 1993;7:2064–2070.
33. Moynagh PN. The roles of Pellino E3 ubiquitin ligases in immunity. *Nat Rev Immunol*. 2014;14:122–131.
34. Tong H, Chen W, Steenbergen C, Murphy E. Ischemic preconditioning activates phosphatidylinositol-3-kinase upstream of protein kinase C. *Circ Res*. 2000;87:309–315.
35. Ding VW, Chen RH, McCormick F. Differential regulation of glycogen synthase kinase 3β by insulin and Wnt signaling. *J Biol Chem*. 2000;275:32475–32481.
36. Thirunavukkarasu M, Han Z, Zhan L, Penumathsa SV, Menon VP, Maulik N. Adeno-sh-β-catenin abolishes ischemic preconditioning-mediated cardioprotection by downregulation of its target genes VEGF, Bcl-2, and survivin in ischemic rat myocardium. *Antioxid Redox Signal*. 2008;10:1475–1484.
37. Shiojima I, Walsh K. Role of Akt signaling in vascular homeostasis and angiogenesis. *Circ Res*. 2002;90:1243–1250.
38. Cardone MH, Roy N, Stennicke HR, Salvesen GS, Franke TF, Stanbridge E, Frisch S, Reed JC. Regulation of cell death protease caspase-9 by phosphorylation. *Science*. 1998;282:1318–1321.
39. Ishii M, Shibata R, Kondo K, Kambara T, Shimizu Y, Tanigawa T, Bando YK, Nishimura M, Ouchi N, Murohara T. Vildagliptin stimulates endothelial cell network formation and ischemia-induced revascularization via an endothelial nitric-oxide synthase-dependent mechanism. *J Biol Chem*. 2014;289:27235–27245.
40. Dimmeler S, Dernbach E, Zeiher AM. Phosphorylation of the endothelial nitric oxide synthase at ser-1177 is required for VEGF-induced endothelial cell migration. *FEBS Lett*. 2000;477:258–262.
41. Pimentel RC, Yamada KA, Kleber AG, Saffitz JE. Autocrine regulation of myocyte Cx43 expression by VEGF. *Circ Res*. 2002;90:671–677.
42. Iyer RK, Odedra D, Chiu LL, Vunjak-Novakovic G, Radisic M. Vascular endothelial growth factor secretion by nonmyocytes modulates connexin-43 levels in cardiac organoids. *Tissue Eng Part A*. 2012;18:1771–1783.
43. Wang DG, Zhang FX, Chen ML, Zhu HJ, Yang B, Cao KJ. Cx43 in mesenchymal stem cells promotes angiogenesis of the infarcted heart independent of gap junctions. *Mol Med Rep*. 2014;9:1095–1102.

Supplemental Material

Figure S1. Evaluation of arteriogenesis with α-smooth muscle actin staining in immunofluorescence images.

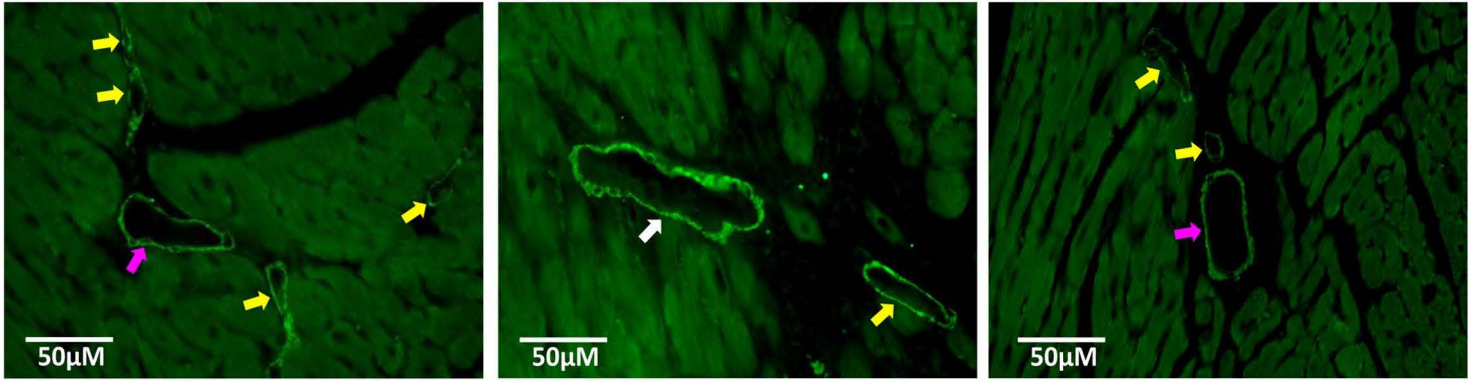

⇨ Yellow Arrow head represents Small vessel 11-50μm in diameter

➡ Pink Arrow represents Medium vessel 50-75μm in diameter

⇨ WhiteThick Arrow represents Large vessel < 75μm in diameter

Representative images show small-, medium- and large-sized arterioles. The yellow arrow represents a small vessel between 11 and 50 μm in diameter; the pink arrow represents a medium vessel between 50 and 75 μm in diameter; the thick white arrow represents a large vessel greater than 75 μm in diameter.

Figure S2. Immunohistochemical analysis of Peli1 fluorescence intensity in heart sections 4 days after injection with Ad-LacZ or Ad-Peli1.

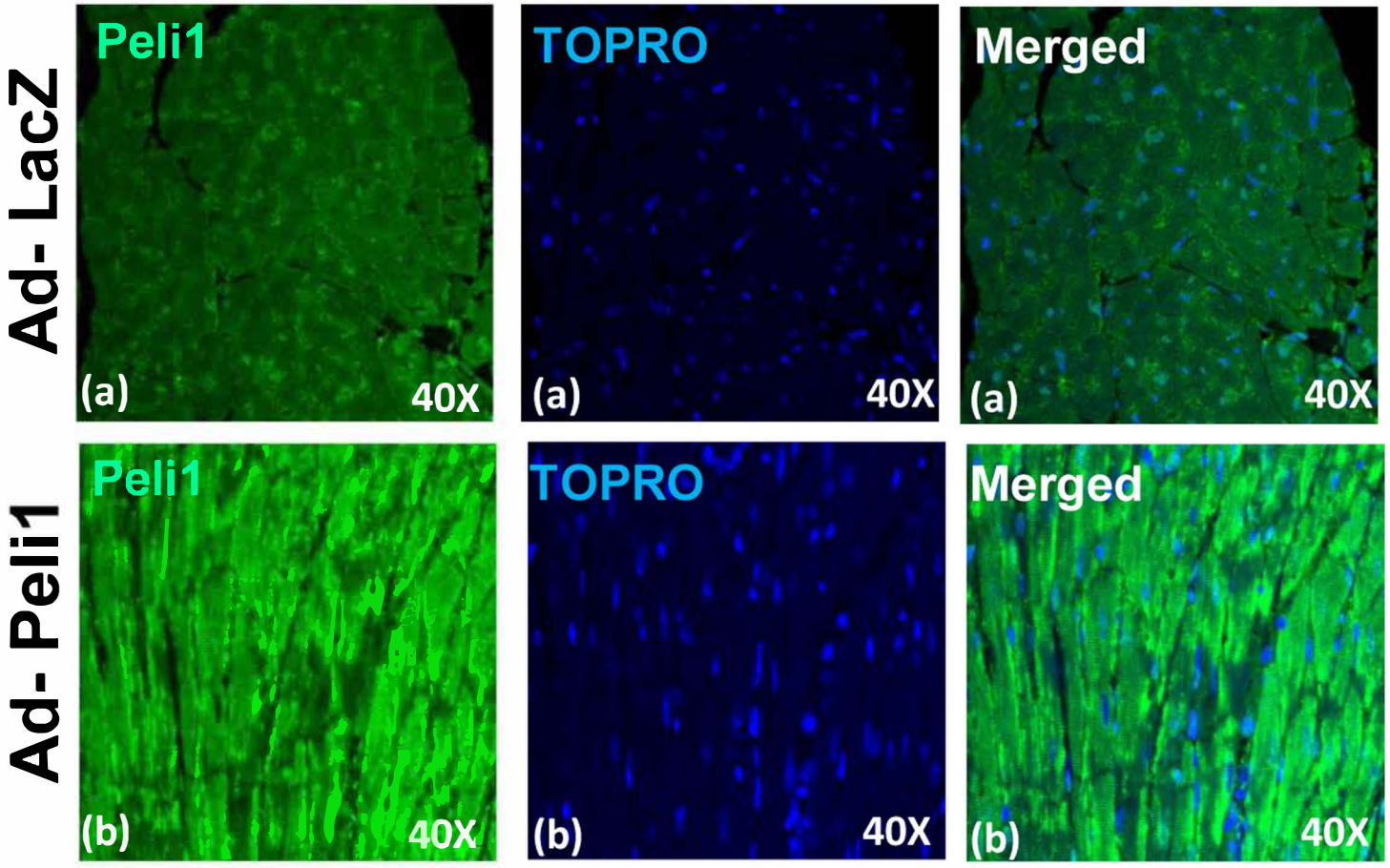

(A) The Ad-LacZ group showed less-intense fluorescence, due to reduced Peli1 expression. **(B)** The Ad-Peli1-treated group showed significantly more intense fluorescence due to increased Peli1 expression. TO-PRO-3 Iodide was used for nuclear staining.